NASA TECHNICAL MEMORANDUM

NASA TM X-64531

STABILITY OF A TWO-DEGREE-OF-FREEDOM SYSTEM WITH STATIC AND IMPULSIVE LOADING

By Mitchell Cash
Central Systems Engineering

July 24, 1970

NASA

George C. Marshall Space Flight Center
Marshall Space Flight Center, Alabama

TECHNICAL REPORT STANDARD TITLE PAGE

1. REPORT NO.	2. GOVERNMENT ACCESSION NO.	3. RECIPIENT'S CATALOG NO.
TM X-64531		

4. TITLE AND SUBTITLE	5. REPORT DATE
Stability of a Two-Degree-of-Freedom System With Static and Impulsive Loading	July 24, 1970
	6. PERFORMING ORGANIZATION CODE
7. AUTHOR(S) Mitchell Cash	8. PERFORMING ORGANIZATION REPORT #
9. PERFORMING ORGANIZATION NAME AND ADDRESS George C. Marshall Space Flight Center Marshall Space Flight Center, Alabama 35812	10. WORK UNIT NO.
	11. CONTRACT OR GRANT NO.
	13. TYPE OF REPORT & PERIOD COVERED Technical Memorandum
12. SPONSORING AGENCY NAME AND ADDRESS	14. SPONSORING AGENCY CODE

15. SUPPLEMENTARY NOTES

Prepared by Central Systems Engineering, Science and Engineering Directorate

16. ABSTRACT

Energy methods are used to determine the stability of a nondimensional two-degree-of-freedom column model under static and impulsive loading. A soft spring is used to create instability, and provision is made for initial imperfections. Stability is investigated at the static buckling load and at the saddles of the deflected system without a static load, and the difference is noted. Solution curves are determined for initial conditions to equal the saddle critical potential energy, and the excess initial energy required for collapse of the system is determined for various conditions. A numerical integration is used to determine the system responses. The effects of the various system parameters on the response are discussed.

17. KEY WORDS	18. DISTRIBUTION STATEMENT
	Public release approved. Mitchell Cash Mitchell Cash

19. SECURITY CLASSIF. (of this report)	20. SECURITY CLASSIF. (of this page)	21. NO. OF PAGES	22. PRICE
Unclassified	Unclassified	64	$3.00

MSFC - Form 3292 (May 1969)

TABLE OF CONTENTS

TABLE OF CONTENTS (Concluded)

LIST OF ILLUSTRATIONS

LIST OF ILLUSTRATIONS (Concluded)

DEFINITION OF SYMBOLS

Symbol	Definition
k	Spring constant of a torsional spring, inch-pounds.
k_l	Spring constant of a linear extensional spring, pounds.
l	Length of link, inches.
m, m_i	Mass, pounds.
$2r$	Length of major axis of an ellipse.
t	Time, seconds.
q_i	Generalized coordinates of model.
y_i, z_i	Rotated set of coordinates.
C	Constant of Euler load = $\frac{3-\sqrt{5}}{2}$.
E	Total energy of the system, inch-pounds.
E_n	Total energy of the nondimensional system.
F	Magnitude of the nondimensional load, $\frac{P}{P_{cr}}$.
I	Magnitude of the nondimensional impulse, $F_D \Delta\tau$.
P	Magnitude of load, pounds.
Q_i	Generalized forces, inch-pounds.
S^2	Dimensionless constant, $\frac{ml^2\omega^2}{k} = \frac{7-\sqrt{41}}{4}$.
T	Kinetic energy, inch-pounds.
T_n	Nondimensional kinetic energy.
U	Potential energy of internal forces or strain energy, inch-pounds.

DEFINITION OF SYMBOLS (Continued)

Symbol	Definition
U_n	Nondimensional potential energy of internal forces.
V	Total potential energy, inch-pounds.
V_n	Nondimensional total potential energy.
β	Arbitrary constant that softens the spring.
δ, Δ	Incremental change in variables.
ϵ_i	Imperfection or eccentricity of links, radians.
η_i	Changed coordinates where $\varphi_i = \frac{\eta_i}{\beta^{1/2}}$.
τ	Nondimensional time, ωt.
φ_1	Angular displacement of lower link from the vertical, radians.
φ_2	Angular displacement of upper link from the vertical, radians.
ψ	Angular rotation of y_i, z_i axes, degrees.
ω	Angular frequency, radians/second.
Ω	Potential energy of external load, inch-pounds.
Ω_n	Nondimensional potential energy of external load.

Superscripts	Definition
$\dot{}$	Derivative of displacement with respect to t.
$\ddot{}$	Second derivative of displacement with respect to t.
$'$	Derivative of displacement with respect to τ.

DEFINITION OF SYMBOLS (Concluded)

Superscripts	Definition
$''$	Second derivative of displacement with respect to τ.
$\wedge$	Initial velocity after impulse.
$-$	Evaluated in the reference state.
$^\circ$	Degree.

Subscripts	Definition
b	Initial energy.
cr	Critical value.
D	Dynamic load.
f	Final energy.
i, j, k, l	Index notation with range of 1 to 2 except as noted.
n	Nondimensional value.
0	Initial condition.
S	Static load.

TECHNICAL MEMORANDUM X-64531

STABILITY OF A TWO-DEGREE-OF-FREEDOM SYSTEM WITH STATIC AND DYNAMIC LOADING

SECTION I. SUMMARY

Energy methods are applied to determine the stability of a nondimensional two-degree-of-freedom column model under static and impulsive loading. A soft spring is used to create instability, and provision is made for initial imperfections. No dissipation force is considered. The principle of minimum potential energy is used to determine stability of the linear system at the critical static buckling load. A two-dimensional potential energy contour plot locates the saddles of the nonlinear deflected system and the critical potential energy of the saddle is determined. Stability at the saddle without a static load is investigated.

The initial kinetic energy to reach the saddles with and without static loading is provided by a pure impulse (initial velocities of the system) or a square-wave impulsive load with an initial imperfection. Solution curves are determined for the various initial conditions. A numerical integration is used to determine the system response and the excess initial kinetic energy required to cause collapse is determined for various conditions.

A relationship is shown between the pure impulse and the impulsive load with imperfections. The difference in stability criterion at the initial static critical buckling load and at the saddle of the deflected system without a static load is noted. The effects of the various system parameters are discussed in the conclusions.

This is an initial investigation of a simplified system. Investigation of more complex systems may lead to application of the methods to physical systems.

SECTION II. INTRODUCTION

A. Buckling

In a broad sense, the theory of buckling is the theory of the stability of equilibrium of mechanical systems. As the load on a mechanical system increases, the equilibrium states trace paths in a configuration space. At some load a "bifurcation point" or fork may be reached, and different paths may be traced from this point. Exceeding this critical (or Euler) load results in buckling, and the initial postbuckling behavior of the system depends on the stability or instability of equilibrium at the critical buckling load.

Most of the phenomena associated with instability and buckling can be observed in simple systems. The one-degree-of-freedom system depicted in Figure 1a illustrates this phenomenon.* It is composed of two rigid bars joined by a frictionless pin, and constrained by a linear extensional spring (k_1) and a torsional spring (k). The top is constrained to move vertically while the bottom is pinned to a fixed support by a frictionless pin.

B. Bifurcation of Equilibrium States

Figure 1b depicts the deflection of the system as a function of a nondimensional load. At the bifurcation point ($P = P_{cr}$) the equilibrium paths branch into the curves 1A or 1B. The horizontal branch depicts the classical theory.

If the extensional spring (k_1) is removed, the equilibrium path is 1A, which represents a stable configuration. This is typical of the actual postbuckling behavior of large bars. If the extensional spring is retained and the torsional spring (k) is removed, the equilibrium path is 1B, which represents unstable configurations. In some types of structures, particularly shells, an instantaneous displacement of considerable magnitude can occur as the structure moves from one point on the equilibrium path to another point on the path. This is known as "snap-through" and is shown in Figure 2.

Imperfection-sensitivity and its effect on static buckling has been studied intensively in recent years. The curves of Figure 3 are based on the studies of Koiter [1], where the solid lines represent the states of

* This model was developed by Dr. G. A. Wempner, University of Alabama in Huntsville.

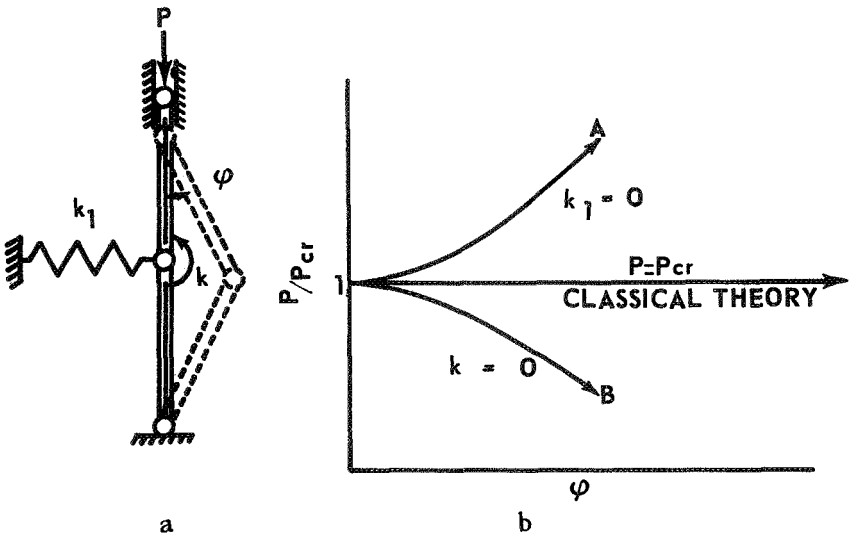

Figure 1. Buckling of a column.

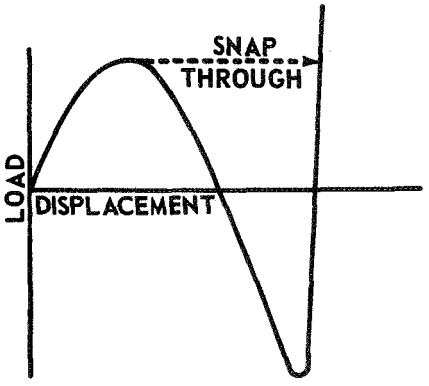

Figure 2. Snap-through.

equilibrium of perfect systems, and the dotted lines represent the states of equilibrium of imperfect systems. Figure 3a represents stable equilibrium as the load must increase with deflection. Figure 3b represents unstable equilibrium as the load decreases with deflection. Figure 3b has greater imperfection sensitivity.

C. Purpose of the Study

The effects of static and dynamic loading on a simplified nondimensional two-degree-of-freedom system are examined to determine whether the methods are applicable to stability analyses. The study contains four parts:

1. A linear analysis to determine the critical conditions for initial buckling.

2. A nonlinear analysis of the potential energy to ascertain the stability of the equilibrium states.

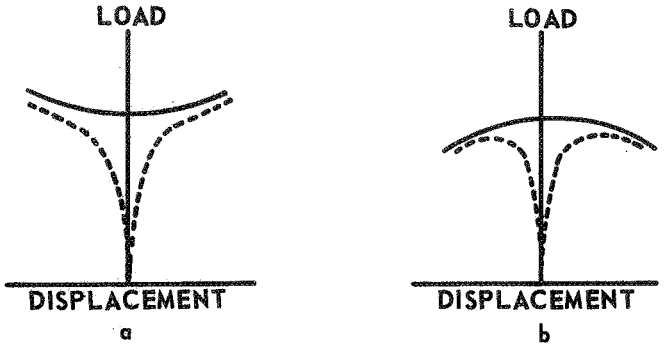

Figure 3. Postbuckling behavior and imperfections.

3. An analysis of the dynamic loading that will cause unrestricted deflections.

4. An analysis of the effect of initial imperfections.

The principle of minimum potential energy and a Taylor series expansion about the equilibrium state are used in the stability analysis. No dissipation force is considered. Lagrange's equations of motion for conservative systems are used in the dynamic analysis with an applied static and/or dynamic load. The initial kinetic energy that will equal the critical potential of the saddle is determined. A numerical integration is then used to determine the excess initial kinetic energy that will result in collapse of the system.

SECTION III. THE MODEL

A. Description of the Model

The two-degree-of-freedom model used in the analyses is shown in Figure 4. It is a double pendulum composed of two rigid weightless bars of equal length, l, which carry two masses such that $m_1 = 2m$ and $m_2 = m$. The pins on which the bars rotate are frictionless. The generalized coordinates are angles φ_1 and φ_2 measured from the vertical. An imperfection, a small angle (ϵ), is provided for each link to determine the effect of imperfections under impulse loading. The restoring force consists of a nonlinear torsional spring at each pin such that the restoring force is of the form

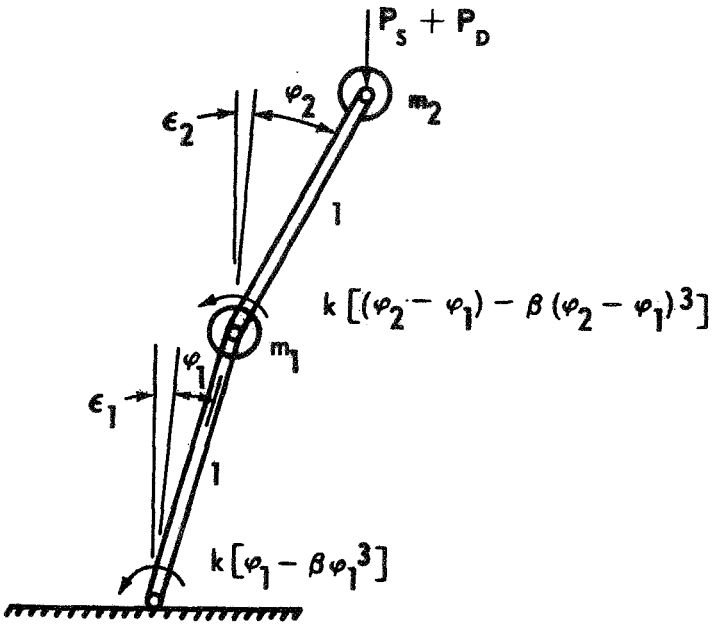

Figure 4. Two-degree-of-freedom model.

$k(\varphi - \beta\varphi^3)$

with β an arbitrary constant. The soft spring is to produce conditions similar to snap-through. A force is applied at the free end of the linkage; this is a conservative static force (P_S) and/or a dynamic force (P_D) where P_D is a function of time. The force of gravity on the masses is neglected.

The kinetic energy, T, the external potential energy, Ω, the internal potential energy, U, and the generalized forces, Q_1 and Q_2, of the system shown in Figure 4 are

$$T = \frac{1}{2} ml^2[3\dot{\varphi}_1^2 + 2\dot{\varphi}_1\dot{\varphi}_2 \cos(\varphi_2 + \epsilon_2 - \varphi_1 - \epsilon_1) + \dot{\varphi}_2^2] \quad , \tag{1a}$$

$$\Omega = P_S l [\cos(\varphi_1 + \epsilon_1) + \cos(\varphi_2 + \epsilon_2) - 2] \quad , \tag{1b}$$

$$U = k\left[\frac{\varphi_1^2}{2} - \beta\frac{\varphi_1^4}{4} + \frac{(\varphi_2 - \varphi_1)^2}{2} - \beta\frac{(\varphi_2 - \varphi_1)^4}{4}\right] \quad , \tag{1c}$$

$$Q_1 = P_D l \sin(\varphi_1 + \epsilon_1) \quad , \tag{1d}$$

$$Q_2 = P_D l \sin(\varphi_2 + \epsilon_2) \quad . \tag{1e}$$

The total potential energy of the system is

$$V = U + \Omega \quad . \tag{2}$$

B. Requirements for Stable Equilibrium

The principle of minimum potential energy states that a conservative holonomic system is in a configuration of stable equilibrium if, and only if, the potential energy is a relative minimum [2]. To examine the requirements for stable equilibrium, let q_i denote the generalized coordinates of the system, with $i = 1, 2$. Then the change in potential energy is

$$\Delta V = V(q_i + \delta q_i) - V(q_i) \quad .$$

Expansion of this in a Taylor series can be written as

$$\Delta V = \delta V + \delta^2 V + \delta^3 V + \delta^4 V + R \tag{3}$$

where δV is known as the first variation, $\delta^2 V$ as the second variation, etc.

The system has a stationary value and is in equilibrium if $\delta V = 0$. This stationary value can be a maximum, a minimum, or a saddle, and the state of stability is determined by the higher order terms of equation (3). Since the potential energy is a relative minimum for stable equilibrium,

$\Delta V > 0$ is necessary and sufficient for stability [1]. A further necessary condition for stability [1] is

$$\delta^2 V \geqq 0 \quad . \tag{4}$$

C. Equations of Equilibrium

For the two-degree-of-freedom system shown in Figure 4, the first variation is

$$\delta V = \frac{\partial V}{\partial \varphi_1} \delta\varphi_1 + \frac{\partial V}{\partial \varphi_2} \delta\varphi_2 \quad .$$

Since $\delta\varphi_1$ and $\delta\varphi_2$ are independent, the equilibrium conditions can be expressed as

$$\frac{\partial V}{\partial \varphi_i} = 0 \quad ,$$

and the equations of equilibrium are

$$-P_S l \sin(\varphi_1 + \epsilon_1) + k\{2\varphi_1 - \varphi_2 - \beta[\varphi_1^3 - (\varphi_2 - \varphi_1)^3]\} = 0 \quad , \tag{5a}$$

$$-P_S l \sin(\varphi_2 + \epsilon_2) + k[\varphi_2 - \varphi_1 - \beta(\varphi_2 - \varphi_1)^3] = 0 \quad . \tag{5b}$$

D. Critical Buckling Load

The second variation, $\delta^2 V$, is a positive definite quadratic when $P < P_{cr}$. With $\delta V = 0$, the second variation is

$$\delta^2 V = \frac{1}{2!} \left(\frac{\partial^2 V}{\partial \varphi_1^2} \delta\varphi_1^2 + 2 \frac{\partial^2 V}{\partial \varphi_1 \partial \varphi_2} \delta\varphi_1 \delta\varphi_2 + \frac{\partial^2 V}{\partial \varphi_2^2} \delta\varphi_2^2 \right) \quad .$$

The right side can be expressed in matrix form as $\Phi \underline{\overline{X}} \Phi^t$, or

$$\delta^2 V = [\delta\varphi_1 \ \delta\varphi_2] \begin{bmatrix} \frac{\partial^2 V}{\partial \varphi_1^2} & \frac{\partial^2 V}{\partial \varphi_1 \partial \varphi_2} \\ \frac{\partial^2 V}{\partial \varphi_1 \partial \varphi_2} & \frac{\partial^2 V}{\partial \varphi_2^2} \end{bmatrix} \begin{bmatrix} \delta\varphi_1 \\ \delta\varphi_2 \end{bmatrix} \tag{6}$$

For other than trivial conditions, the character of equation (6) is determined by the matrix $\underline{\overline{X}}$. At the critical buckling load, the matrix $\underline{\overline{X}}$ becomes positive semidefinite [2] and

$$\det \underline{\overline{X}} = 0 \quad .$$

In determining the critical buckling load of the perfect system, ϵ_i is neglected. The higher order terms of φ_i are also neglected since near $\varphi_1 = \varphi_2 = 0$ these are much smaller than φ_1 and φ_2. Substitution of equations (1b), (1c), and (2) into equation (6) and setting $\det \underline{\overline{X}} = 0$ yields

$$\begin{vmatrix} -Pl + 2k & -k \\ -k & -Pl + k \end{vmatrix} = 0 \quad .$$

Solution of this gives

$$P = \left(\frac{3 \pm \sqrt{5}}{2} \right) \frac{k}{l} \quad ,$$

and the lower value is the critical or Euler buckling load

$$P_{cr} = \left(\frac{3 - \sqrt{5}}{2} \right) \frac{k}{l} \tag{7}$$

E. Initial Buckling Mode

To determine the initial buckling mode, P_{cr} is substituted for P in equation (5a) or (5b), again neglecting higher orders of φ_i. Equation (5a) then gives the initial buckling mode as

$$\delta\varphi_2 = \left(\frac{1+\sqrt{5}}{2}\right)\delta\varphi_1 \quad . \tag{8}$$

F. Equations of Motion

Since the system of Figure 4 is holonomic, the nonlinear equations of motion are given by Lagrange's equations [3] as

$$\frac{d}{dt}\left(\frac{\partial T}{\partial \dot{\varphi}_i}\right) - \frac{\partial T}{\partial \varphi_i} + \frac{\partial V}{\partial \varphi_i} = Q_i \quad .$$

Substitution of equation (1) into this gives

$$\begin{aligned} &m l^2[3\ddot{\varphi}_1 + \ddot{\varphi}_2 \cos(\varphi_2 + \epsilon_2 - \varphi_1 - \epsilon_1) - \dot{\varphi}_2^2 \sin(\varphi_2 + \epsilon_2 - \varphi_1 - \epsilon_1)] \\ &+ k\{2\varphi_1 - \varphi_2 - \beta[\varphi_1^3 - (\varphi_2 - \varphi_1)^3]\} = (P_S + P_D)\, l \sin(\varphi_1 + \epsilon_1) \quad , \end{aligned} \tag{9a}$$

$$\begin{aligned} &m l^2[\ddot{\varphi}_2 + \ddot{\varphi}_1 \cos(\varphi_2 + \epsilon_2 - \varphi_1 - \epsilon_1) + \dot{\varphi}_1^2 \sin(\varphi_2 + \epsilon_2 - \varphi_1 - \epsilon_1)] \\ &+ k[\varphi_2 - \varphi_1 - \beta(\varphi_2 - \varphi_1)^3] = (P_S + P_D)\, l \sin(\varphi_2 + \epsilon_2) \end{aligned} \tag{9b}$$

To determine the linear frequency equation with $P_D = 0$, assume solutions of equation (9) in the form of

$$\varphi_i = A_i \sin(\omega t + \Lambda)$$

with $\varphi_1 << 1$ and $\varphi_2 << 1$, which yields

$$(-3ml^2\omega^2 + 2k - P_S l)\, A_1 + (-ml^2\omega^2 - k)\, A_2 = 0 \quad ,$$

$$(-ml^2\omega^2 - k)\, A_1 + (-ml^2\omega^2 + k - P_S l)\, A_2 = 0 \quad .$$

This has a nontrivial solution only if the determinant of the coefficients of A_1 and A_2 vanish. Let

$$\frac{ml^2\omega^2}{k} = S^2 \quad \text{and} \quad \frac{P_S l}{k} = N \quad .$$

The frequency equation is then

$$2S^4 + (4N - 7)\, S^2 + (N^2 - 3N + 1) = 0 \tag{10}$$

If $P_S = 0$, this reduces to

$$2S^4 - 7S^2 + 1 = 0$$

and

$$S^2 = \frac{7 \pm \sqrt{41}}{4} \quad .$$

The lowest natural frequency of the linear system is then

$$S^2 = \frac{7 - \sqrt{41}}{4} \quad . \tag{11}$$

To determine the critical load of the linear system, let $\omega = 0$. Then $S^2 = 0$ and equation (16) becomes

$$N^2 - 3N + 1 = 0 \quad ,$$

and

$$N = \frac{P_S l}{k} = \frac{3 \pm \sqrt{5}}{2} \quad .$$

The critical or buckling load is the lower value

$$P_{cr} = \left(\frac{3 - \sqrt{5}}{2}\right) \frac{k}{l}$$

which agrees with equation (7).

G. Nondimensional Equations

To eliminate certain physical parameters, the equations of motion are changed to a nondimensional form by using the dimensionless quantities:

$$S^2 = \frac{ml^2\omega^2}{k} \quad , \tag{12a}$$

$$F_S = \frac{P_S}{P_{cr}} \quad , \tag{12b}$$

$$\tau = \omega t \quad . \tag{12c}$$

With $\varphi' = \omega\dot{\varphi}$ and $\varphi'' = \omega^2\ddot{\varphi}$, the nondimensional equations of motion are

$$S^2[3\varphi_1'' + \varphi_2'' \cos(\varphi_2 + \epsilon_2 - \varphi_1 - \epsilon_1) - (\varphi_2')^2 \sin(\varphi_2 + \epsilon_2 - \varphi_1 - \epsilon_1)] + \{2\varphi_1 - \varphi_2 - \beta[\varphi_1^3 - (\varphi_2 - \varphi_1)^3]\} = CF \sin(\varphi_1 + \epsilon_1) \quad , \tag{13a}$$

$$S^2[\varphi_2'' + \varphi_1'' \cos(\varphi_2 + \epsilon_2 - \varphi_1 - \epsilon_1) + (\varphi_1')^2 \sin(\varphi_2 + \epsilon_2 - \varphi_1 - \epsilon_1)] + \{\varphi_2 - \varphi_1 - \beta(\varphi_2 - \varphi_1)^3\} = CF \sin(\varphi_2 + \epsilon_2) \quad , \tag{13b}$$

where $S^2 = \frac{7 - \sqrt{41}}{4}$, $C = \frac{3 - \sqrt{5}}{2}$, and F is defined as F_D and/or F_S.

The nondimensional equations of equilibrium are

$$2\varphi_1 - \varphi_2 - \beta[\varphi_1^3 - (\varphi_2 - \varphi_1)^3] - CF_S \sin(\varphi_1 + \epsilon_1) = 0 \quad , \tag{14a}$$

$$\varphi_2 - \varphi_1 - \beta(\varphi_2 - \varphi_1)^3 - CF_S \sin(\varphi_2 + \epsilon_2) = 0 \quad . \tag{14b}$$

The nondimensional energy equation is

$$\begin{aligned} E_n = \frac{S^2}{2} & [3(\varphi_1')^2 + 2\varphi_1' \varphi_2' \cos(\varphi_2 + \epsilon_2 - \varphi_1 - \epsilon_1) + (\varphi_2')^2] \\ & + CF_S[\cos(\varphi_1 + \epsilon_1) + \cos(\varphi_2 + \epsilon_2) - 2] \\ & + \frac{1}{4}[2\varphi_1^2 - \beta\varphi_1^4 + 2(\varphi_2 - \varphi_1)^2 - \beta(\varphi_2 - \varphi_1)^4] \quad , \end{aligned} \tag{15a}$$

where

$$E_n = T_n + \Omega_n + U_n \quad . \tag{15b}$$

The remainder of the analyses is based on the nondimensional equations. In these, the critical buckling load is

$$F_{cr} = 1 \quad . \tag{16}$$

SECTION IV. EQUILIBRIUM

A. Stable Equilibrium

At the critical buckling load, equation (4) becomes zero, and the necessary conditions for stable equilibrium [1] are

$$\delta^3 V = 0$$

$$\delta^4 V \geq 0 \quad .$$

The third variation is identically zero, due to the symmetry of the model. Therefore, the fourth variation must be positive definite for stable equilibrium, or

$$\delta^4 V = \frac{1}{4!}\left(\frac{\partial^4 V}{\partial \varphi_1^4}\,\delta\varphi_1^4 + 4\,\frac{\partial^4 V}{\partial \varphi_1^3\,\partial \varphi_2}\,\delta\varphi_1^3\,\delta\varphi_2 + 6\,\frac{\partial^4 V}{\partial \varphi_1^2\,\partial \varphi_2^2}\,\delta\varphi_1^2\,\delta\varphi_2^2 + 4\,\frac{\partial^4 V}{\partial \varphi_1\,\partial \varphi_2^3}\,\delta\varphi_1\,\delta\varphi_2^3 + \frac{\partial^4 V}{\partial \varphi_2^4}\,\delta\varphi_2^4\right) > 0 \quad . \tag{17}$$

Using equation (15), setting $F = F_{cr} = 1$, linearizing at buckling for φ_1 and $\varphi_2 << 1$, and making use of the initial buckling mode of equation (8), equation (17) is found to be

$$\frac{1}{24}\left[(2C - 24\beta)\,\delta\varphi_1^4 + 48\beta\left(\frac{1+\sqrt{5}}{2}\right)\delta\varphi_1^4 - 72\beta\left(\frac{1+\sqrt{5}}{2}\right)^2\delta\varphi_1^4 + 48\beta\left(\frac{1+\sqrt{5}}{2}\right)^3\delta\varphi_1^4 + (2C - 12\beta)\left(\frac{1+\sqrt{5}}{2}\right)^4\delta\varphi_1^4\right] > 0 \quad , \tag{18}$$

where $C = \frac{3-\sqrt{5}}{2}$. Solution of this shows that the system is in stable equilibrium if

$$\beta < \frac{3+\sqrt{5}}{12} \quad \text{or} \quad \beta < 0.4363\ldots \tag{19}$$

The critical value of β is therefore defined as

$$\beta_{cr} = \frac{3+\sqrt{5}}{12} \quad . \tag{20}$$

Because of the symmetry of the model, $\delta^4 V > 0$ as developed in equations (18) and (19) meets the sufficiency condition for stable equilibrium. This is shown in Reference 4.

B. Equilibrium Paths

To determine the equilibrium paths at bifurcation, equation (14) is evaluated at the critical buckling load with an approximation procedure. This consists of linearizing in terms of small changes in the variables. Then the load change that occurs with small finite displacements of the system can be evaluated. Let equation (14) be represented by

$$f_i(\varphi_1, \varphi_2, F) = 0, \quad i = 1, 2 \quad .$$

With an increment in the variables, the corresponding increment in f_i is

$$\Delta f_i = \frac{\partial f_i}{\partial \varphi_1} \delta\varphi_1 + \frac{\partial f_i}{\partial \varphi_2} \delta\varphi_2 + \frac{\partial f_i}{\partial F} \delta F \, , \quad i = 1, 2 \quad .$$

where the derivatives are evaluated in the reference state $(\overline{\varphi}_1, \overline{\varphi}_2, \overline{F})$. Since the system remains in equilibrium,

$$\frac{\partial f_i}{\partial \varphi_1} \delta\varphi_1 + \frac{\partial f_i}{\partial \varphi_2} \delta\varphi_2 + \frac{\partial f_i}{\partial F} \delta F = 0, \quad i = 1, 2 \quad .$$

Substituting equation (14) into this gives

$$\{2 - 3\beta[\overline{\varphi}_1^2 + (\overline{\varphi}_2 - \overline{\varphi}_1)^2] - C\overline{F}_S \cos(\overline{\varphi}_1 + \epsilon_1)\} \delta\varphi_1 + [-1 + 3\beta(\overline{\varphi}_2 - \overline{\varphi}_1)^2] \delta\varphi_2 - [C \sin(\overline{\varphi}_1 + \epsilon_1)] \delta F_S = 0 \, , \tag{21a}$$

$$[-1 + 3\beta(\overline{\varphi}_2 - \overline{\varphi}_1)^2] \delta\varphi_1 + [1 - 3\beta(\overline{\varphi}_2 - \overline{\varphi}_1)^2 - CF_S \cos(\overline{\varphi}_2 + \epsilon_2)] \delta\varphi_2 - [C \sin(\varphi_2 + \epsilon_2)] \delta F_S = 0 \quad . \tag{21b}$$

This is placed in the form

$$A_{11}\,\delta\varphi_1 + A_{12}\,\delta\varphi_2 = A_{13}\,\delta F \quad ,$$

$$A_{21}\,\delta\varphi_1 + A_{22}\,\delta\varphi_2 = A_{23}\,\delta F \quad .$$

Transposing and using Cramer's rule, this can be solved in terms of either $\delta\varphi_1$ or $\delta\varphi_2$; that is,

$$\delta\varphi_2 = \frac{(A_{13}A_{22} - A_{12}A_{23})\,\delta\varphi_1}{D} \quad , \tag{22a}$$

$$\delta F = \frac{-(A_{11}A_{22} + A_{12}A_{21})\,\delta\varphi_1}{D} \quad , \tag{22b}$$

$$D = A_{13}A_{21} - A_{11}A_{23} \quad . \tag{22c}$$

To trace the equilibrium paths, equation (21) was programmed on the SDS930 using the form of equation (22). It is necessary to assign an arbitrary ϵ_1 or ϵ_2 to make equations (21a) or (21b) nonhomogeneous. The program was run for various values of β using $\delta\varphi_1 = 0.0001$ and $\epsilon_1 = 0.01$. The results, as shown in Figure 5, indicate that, with $\beta < \beta_{cr}$ [equation (20)], the system is in stable equilibrium as the load must increase with deflection. With $\beta > \beta_{cr}$, the load decreases with deflection and the system at buckling is in unstable equilibrium. These correspond to the conditions depicted in Figures 3a and 3b, respectively. The unstable system ($\beta > \beta_{cr}$) corresponds to the "snap-through" of shells described in Section II.B.

C. Internal Potential Energy of the System

The strain energy is a nonlinear function of φ_1 and $(\varphi_2 - \varphi_1)$, and the total strain energy is the sum of the strain energies of the two springs. From equation (15), the nondimensional strain energy is

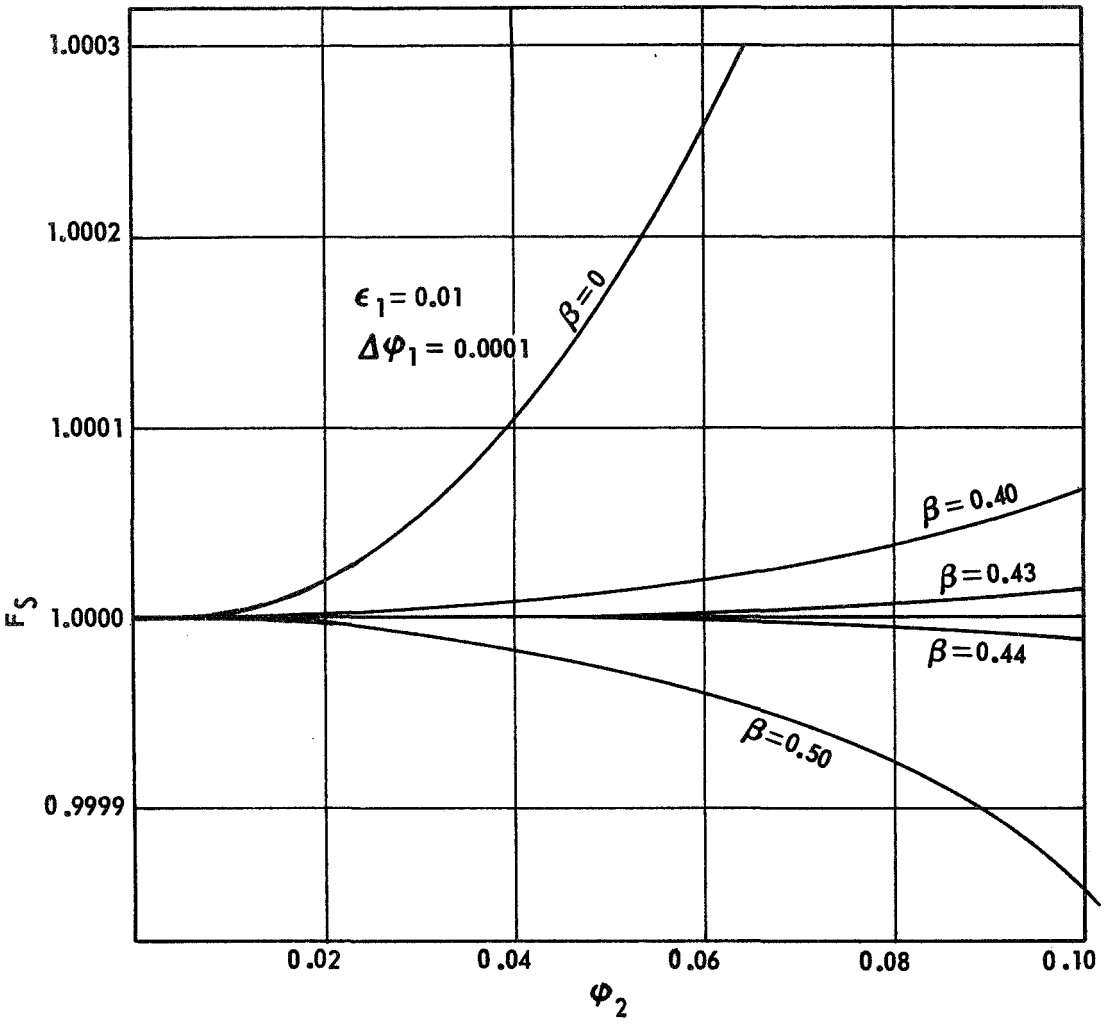

Figure 5. Equilibrium paths at bifurcation.

$$U_n = \frac{1}{4}\left[2\varphi_1^2 - \beta\varphi_1^4 + 2(\varphi_2 - \varphi_1)^2 - \beta(\varphi_2 - \varphi_1)^4\right] \quad . \tag{23}$$

The stationary values for φ_1 and $(\varphi_2 - \varphi_1)$ in equation (23) are found by taking

$$\frac{\partial U_n}{\partial \varphi_1} = \frac{\partial U_n}{\partial(\varphi_2 - \varphi_1)} = 0 \quad ,$$

and the maximum value of U_n in each spring is found to occur at

$$\varphi_1 = \frac{1}{\sqrt{\beta}} \quad \text{and} \quad \varphi_2 - \varphi_1 = \frac{1}{\sqrt{\beta}} \quad . \tag{24}$$

The energy plot of the strain energy of each spring is shown in Figure 6.

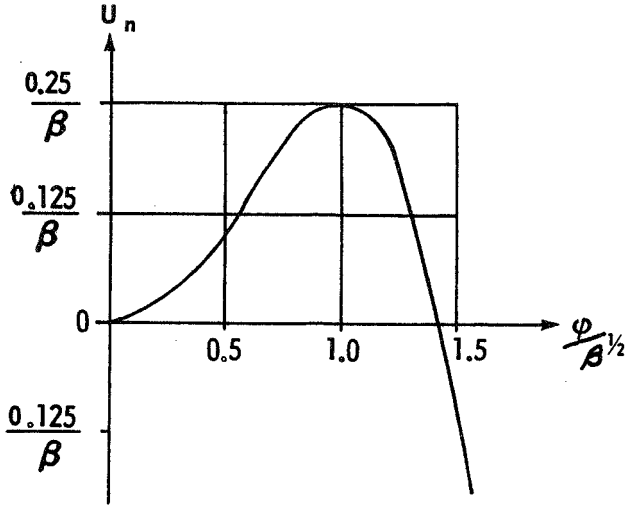

Figure 6. Strain energy of the soft spring.

Since equation (24) shows that the maximum value of the strain energy is an inverse function of $\sqrt{\beta}$, the equilibrium equations are modified by the use of

$$\varphi_i = \frac{\eta_i}{\sqrt{\beta}} \quad , \quad i = 1, 2 \quad , \tag{25}$$

and the equations of equilibrium in the η_i coordinates are

$$2\eta_1 - \eta_1^3 - \eta_2 + (\eta_2 - \eta_1)^3 - CF_S \beta^{1/2} \sin \frac{\eta_1}{\beta^{1/2}} = 0 \quad , \tag{26a}$$

$$\eta_2 - \eta_1 - (\eta_2 - \eta_1)^3 - CF_S \beta^{1/2} \sin \frac{\eta_2}{\beta^{1/2}} = 0 \quad , \tag{26b}$$

where ϵ_i has been neglected because $\epsilon_i << \eta_i$. The strain energy is

$$U_n = \frac{1}{4\beta} [2\eta_1^2 - \eta_1^4 + 2(\eta_2 - \eta_1)^2 - (\eta_2 - \eta_1)^4] \quad .$$

The total spring potential energy of the system is shown in Figure 7 as a two-dimensional plot of equal energy contours. It can be seen that the potential energy is a minimum at the origin where the system is in stable equilibrium, and that there are four saddle points at

$$(1, 0), \quad (0, 1), \quad (-1, 0), \quad (0, -1), \tag{27}$$

which are labeled positions I, II, III, and IV, respectively, for ready reference. The saddle points in the φ coordinates are found by dividing these by $\beta^{1/2}$.

The potential energy contour plot of Figure 7 is important in the analysis of the system. If the system is released from rest at any point (or arrives at that point with no kinetic energy), it will move in the direction of a lower potential. If it is outside the saddle point energy contour in a region of lower potential, the rotation of the system will increase uncontrollably. This is considered to be collapse of the system.

With a large β (very soft spring), the saddle points are near the origin and the system may collapse with small deflections. As β decreases, the saddle points move out (the actual saddle point for $F_S = 0$ is $\varphi_1 = (\varphi_2 - \varphi_1) = 0.111 \ldots$ radians for $\beta = 9.0$, and $1.291 \ldots$ radians for $\beta = 0.6$). At $\beta = 0$, which corresponds to a linear spring, the saddle points are at infinity.

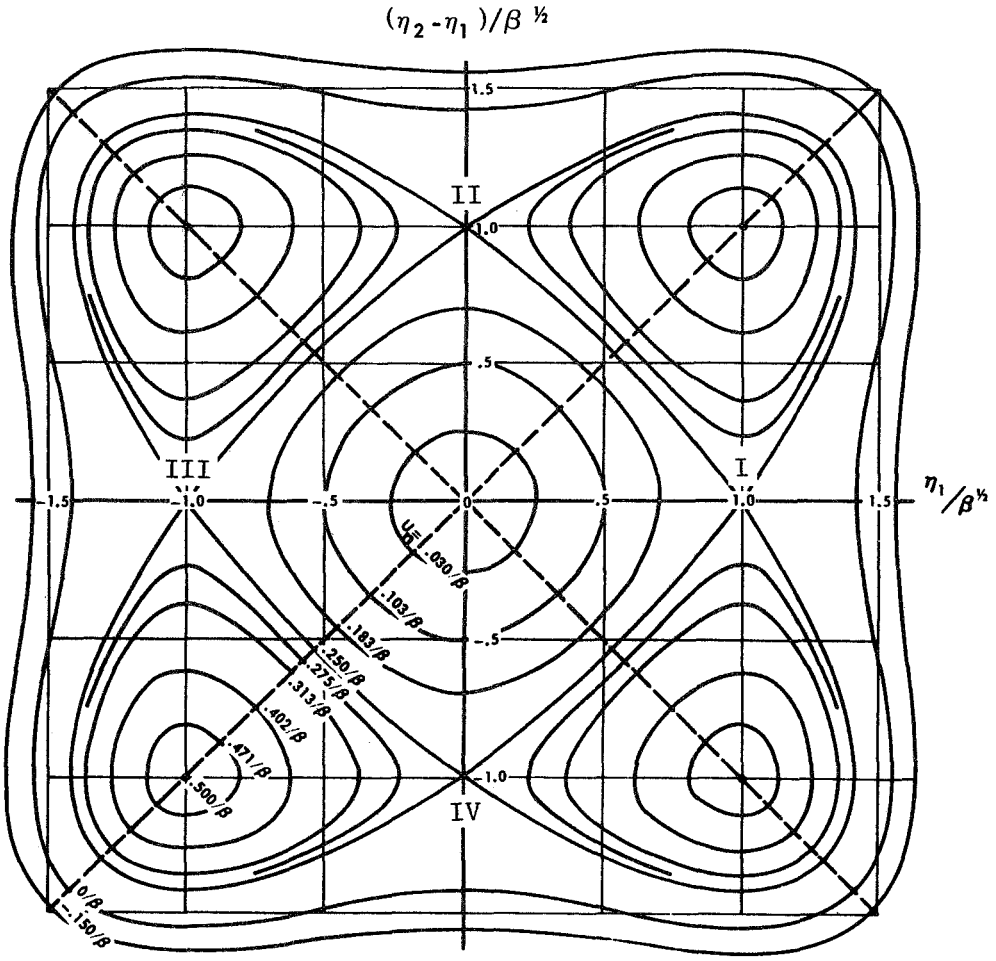

Figure 7. Potential energy contour plot of the spring energy.

D. Change in Saddle Points Under External Loading

The saddle points determined in Section IV.C were based on the internal spring energy only. As an external load is added, the location of these saddles will change. At the saddle points for any specified value of F_S, the system can be represented by the equilibrium equations

$$f_i(\overline{\eta}_1, \overline{\eta}_2, \overline{F}) = 0, \quad i = 1, 2 \quad .$$

The incremental change remains in equilibrium, and

$$\frac{\partial f_i}{\partial \eta_i}\ \delta\eta_1 + \frac{\partial f_i}{\partial \eta_2}\ \delta\eta_2 + \frac{\partial f_i}{\partial F}\ \delta F = 0, \quad i = 1, 2 \quad . \tag{28}$$

Substitution of equation (26) into equation (28) gives

$$\left[\ 2 - 3\overline{\eta}_1^2 - 3(\overline{\eta}_2 - \overline{\eta}_1)^2 - C\overline{F}_S \cos \frac{\overline{\eta}_1}{\beta^{1/2}}\ \right] \delta\eta_1$$

$$+ [3(\overline{\eta}_2 - \overline{\eta}_1)^2 - 1]\ \delta\eta_2 = \left[C\,\beta^{1/2} \sin \frac{\overline{\eta}_1}{\beta^{1/2}} \right] \delta F_S \quad ,$$

$$[3(\overline{\eta}_2 - \overline{\eta}_1)^2 - 1]\ \delta\eta_1 + \left[\ 1 - 3(\overline{\eta}_2 - \overline{\eta}_1)^2 - CF_S \cos \frac{\overline{\eta}_2}{\beta^{1/2}}\ \right] \delta\eta_2$$

$$= \left[C\,\beta^{1/2} \sin \frac{\overline{\eta}_2}{\beta^{1/2}} \right] \delta F_S \quad ,$$

where $\overline{\eta}_i$ and $\overline{F}_S$ are evaluated in the reference state. Since these are linear in $\delta\eta_1$, $\delta\eta_2$, and δF_S, they can be solved by Cramer's rule. Changing the form to

$$B_{11}\ \delta\eta_1 + B_{12}\ \delta\eta_2 = B_{13}\ \delta F_S \quad ,$$

$$B_{21}\ \delta\eta_1 + B_{22}\ \delta\eta_2 = B_{23}\ \delta F_S \quad ,$$

the solution becomes

$$\delta\eta_1 = \frac{(B_{13}B_{22} - B_{12}B_{23})}{D}\ \delta F_S \quad ,$$

$$\delta\eta_2 = \frac{(B_{11}B_{23} - B_{13}B_{21})}{D}\ \delta F_S \quad ,$$

$$D = B_{11}B_{22} - B_{12}B_{21} \quad .$$

Substitution of the saddle point values into the above gives the initial incremental changes in η_1 and η_2 for an incremental external load. The initial changes are depicted in Figure 8.

Figure 8 shows that the changes in the saddle points of positions I and III are mirror images about the axes, as are the changes in positions II and IV. This is because of the symmetry of the model and the oddness of the sine function. The table of Figure 8 also shows that the direction of the saddle point movement reverses when $\beta < \frac{1}{\pi^2}$, a value less than β_{cr} [equation (20)]. Thus, the system becomes unstable under these conditions at a different value of β. The relation between $\sin \frac{\eta}{\beta^{1/2}}$ and β is shown in Figure 9.

It is to be expected that the locus of the saddle points, as F_S increases, will trace a path from at least two of the mirror image positions of Figure 8 to the origin. As the saddle point approaches the origin, it is also expected that

$$\lim_{\eta_1,\ \eta_2 \to 0} F_S = F_{cr} = 1 \quad .$$

Linearizing equation (26) for η_1 and η_2 near zero gives

$$2\eta_1 - \eta_2 = CF_S\ \eta_1 \quad ,$$

$$\eta_2 - \eta_1 = CF_S\ \eta_2 \quad .$$

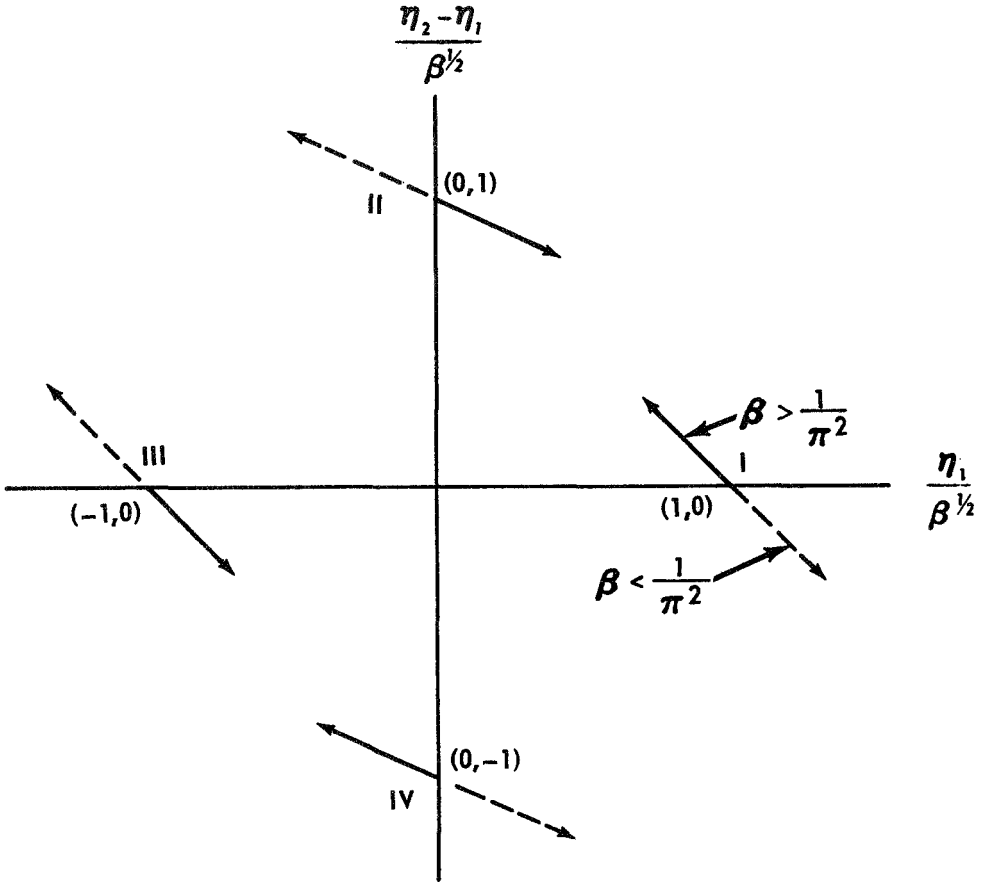

Position	η_1	η_2	$\delta\eta_1$	$\delta\eta_2$	$\delta\eta_2 - \delta\eta_1$
I	1	1	$-C\beta^{1/2}\ \delta F_S \sin \frac{1}{\beta^{1/2}}$	0	$C\beta^{1/2}\ \delta F_S \sin \frac{1}{\beta^{1/2}}$
II	0	1	$C\beta^{1/2}\ \delta F_S \sin \frac{1}{\beta^{1/2}}$	$\frac{1}{2} C\beta^{1/2}\ \delta F_S \sin \frac{1}{\beta^{1/2}}$	$-\frac{1}{2} C\beta^{1/2}\ \delta F_S \sin \frac{1}{\beta^{1/2}}$
III	-1	-1	$-C\beta^{1/2}\ \delta F_S \sin \frac{-1}{\beta^{1/2}}$	0	$C\beta^{1/2}\ \delta F_S \sin \frac{-1}{\beta^{1/2}}$
IV	0	-1	$C\beta^{1/2}\ \delta F_S \sin \frac{-1}{\beta^{1/2}}$	$\frac{1}{2} C\beta^{1/2}\ \delta F_S \sin \frac{-1}{\beta^{1/2}}$	$-\frac{1}{2} C\beta^{1/2}\ \delta F_S \sin \frac{-1}{\beta^{1/2}}$

Figure 8. Change in saddle points with incremental loading.

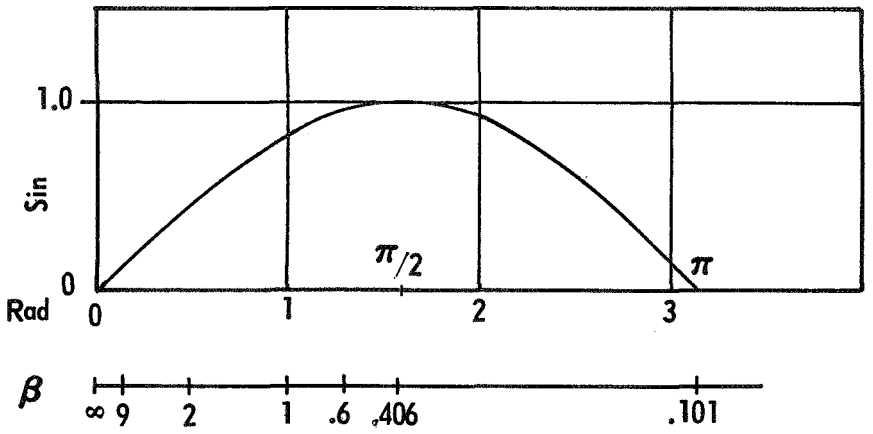

Figure 9. Relation of $\sin \frac{\eta}{\beta^{1/2}}$ and β.

Then as η_1 and $\eta_2 \rightarrow 0$,

$$F_S \rightarrow \frac{2}{C} - \frac{\eta_2}{C\eta_1} \quad , \tag{29a}$$

$$F_S \rightarrow \frac{1}{C} - \frac{\eta_1}{C\eta_2} \quad . \tag{29b}$$

Eliminating $\frac{\eta_2}{\eta_1}$ from equation (29) and solving the resultant quadratic shows that at $\eta_1 = \eta_2 = 0$,

$$\lim_{\eta_1,\, \eta_2 \rightarrow 0} F_S = 1 = F_{cr} \quad .$$

E. Locus of Saddle Points

There are two ways of determining the locus of saddle points as F_S varies from 0 to 1. One is a direct solution of equation (26) for various values of F_S. The other is to eliminate F_S from equation (26), which gives a single equation represented by

$$f(\eta_1, \eta_2, \beta^{1/2}) = 0 \tag{30}$$

where β is an arbitrary constant. From this it can be seen that the solution is a family of curves for various values of β. When equation (30) has been solved for η_1 and η_2, the values can be substituted into equation (26) to determine F_S.

The solutions of equation (26) for values of $\beta = 0.6$ and $\beta = 9.0$ are shown in Figure 10 for the change in saddle point of position I. The change in position III is a mirror image of this. The locus of saddle points from positions II and IV do not approach the origin because η_2 is increasing more rapidly than η_1. Figure 10 also shows that the solution curves do not vary much for widely spread values of β, but that there is some difference in the location of the saddle point for the same values of F_S.

F. Saddle Point Equal Energy Contours

As F_S increases from zero and the saddle points change as shown in Figure 10, the entire potential energy contour plot of Figure 7 will change. Using equation (25) to express the energy in terms of η_1 and η_2 yields

$$E_n = \frac{S^2}{2\beta}\left[3(\eta_1')^2 + 2\eta_1'\eta_2' \cos\frac{(\eta_2-\eta_1)}{\beta^{1/2}} + (\eta_2')^2\right] + CF_S\left(\cos\frac{\eta_1}{\beta^{1/2}} + \cos\frac{\eta_2}{\beta^{1/2}} - 2\right) + \frac{1}{4\beta}\left[2\eta_1^2 - \eta_1^4 + 2(\eta_2-\eta_1)^2 - (\eta_2-\eta_1)^4\right] \tag{31}$$

where ϵ has been neglected because $\epsilon_i \ll \eta_i$. Then the potential energy of the external load and the internal springs can be calculated for any load and position. Using the values of η_1, η_2, and F_S that were the basis of Figure 10, the saddle point equal energy contour lines were calculated for $F_S = 0$, 0.5, and 0.9, and are shown in Figure 11 for a $\beta = 0.6$. Contour lines for saddle points of other values of F_S would lie in between these and be of the same general shape.

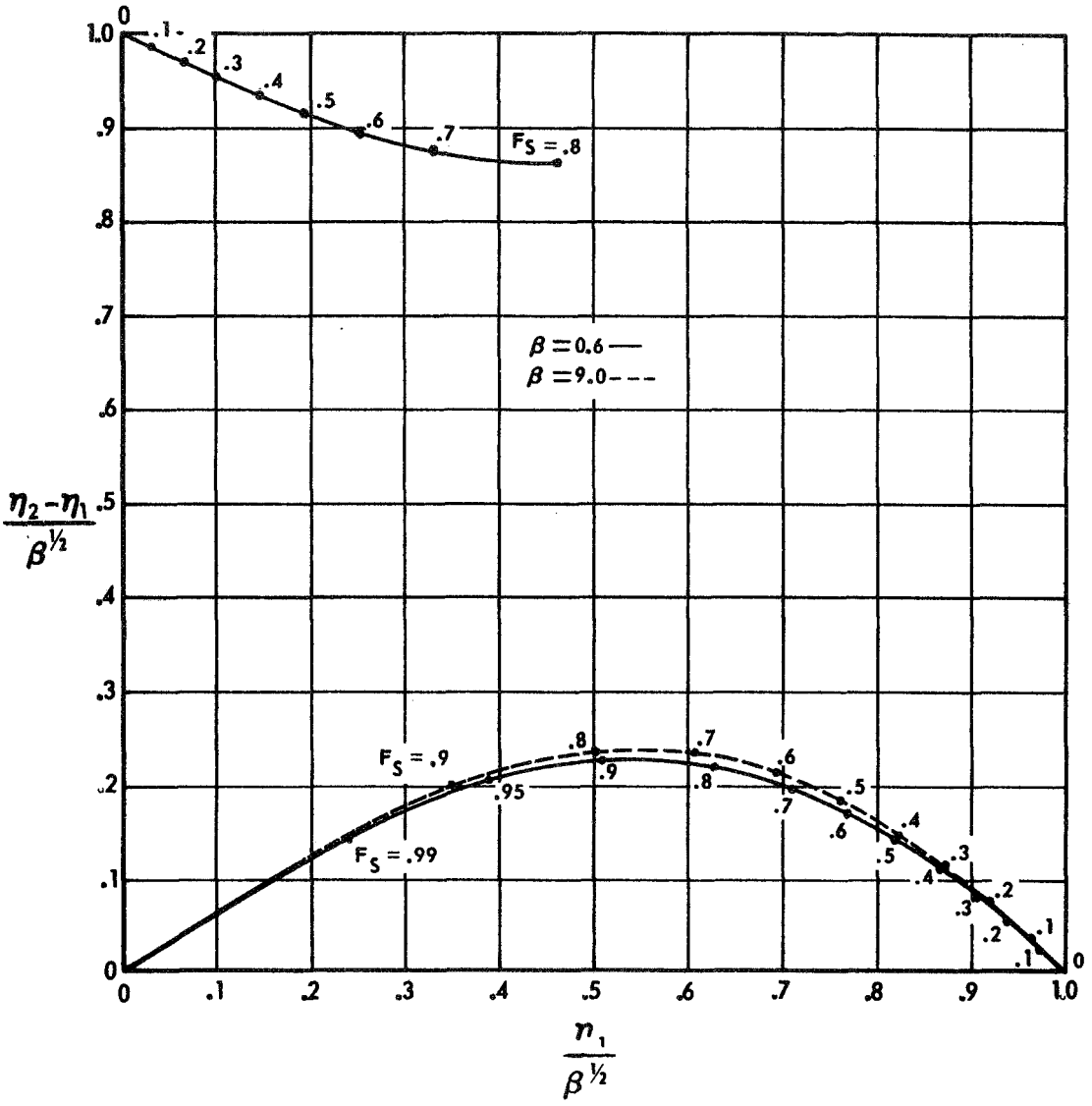

Figure 10. Saddle point location for values of F_S.

The change in saddle points of positions II and IV as F_S increases moves these points outside of the contour $V_n = \frac{0.25}{\beta^{1/2}}$ of Figure 7. They are still saddle points, but at a higher energy level than the saddle points of positions I and III.

The F_S contour lines of Figure 11 have the same significance as those for $F_S = 0$ discussed in Section IV.C. The system without kinetic

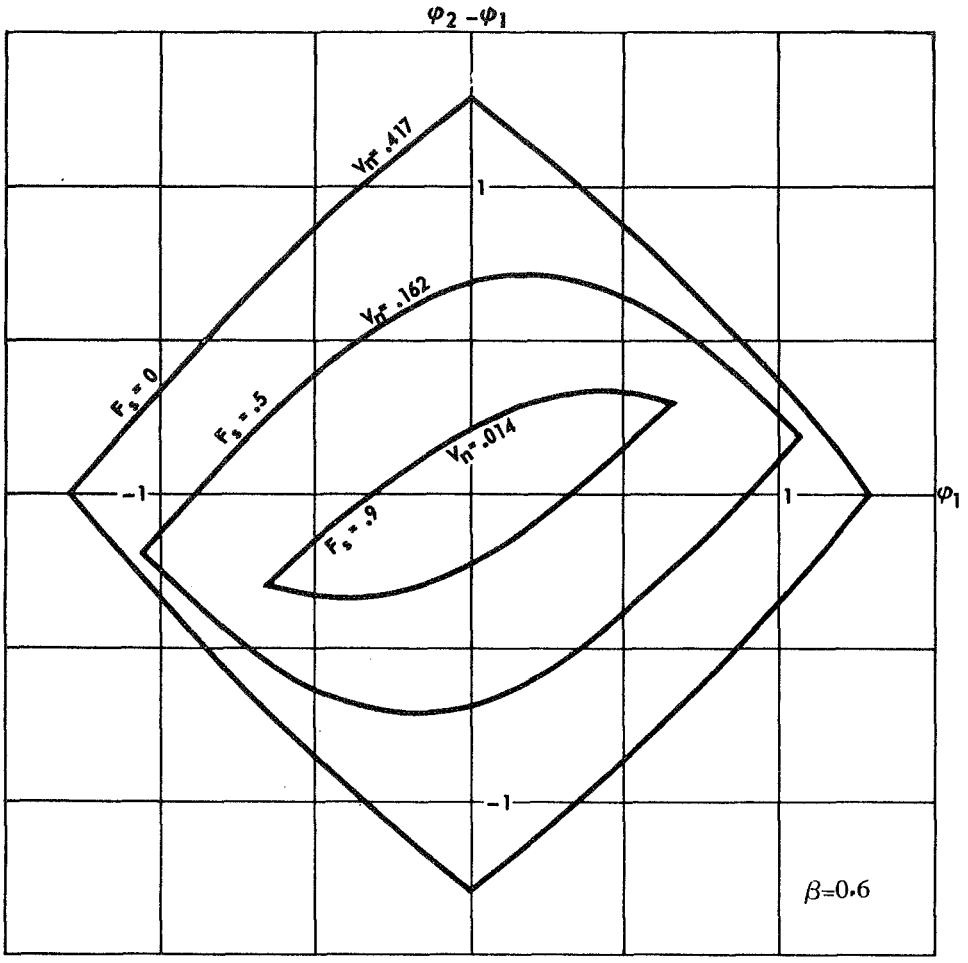

Figure 11. Saddle point potential energy contour plot with F_S.

energy will seek a lower potential energy level. If it is in a region outside the saddle point energy contour for that F_S and at a lower potential than the saddle point, the system will collapse.

G. Critical Potential Energy

Using equation (31) and the values of η_1, η_2, and F_S that determined Figure 10, the potential energy of the system can be calculated at the saddle points. Then the critical potential energy is

$$V_{cr} = U_n + \Omega_n F_S \tag{32}$$

where U_n is the strain energy of the system at the saddle point corresponding to F_S, and Ω_{nF_S} is the potential energy of that static load. Then, V_{cr} is the energy that must be added to the system when $\varphi_1 = \varphi_2 = 0$ to bring the system to the saddle point energy level. Figure 12 shows V_{cr} for $\beta = 0.6$ and $\beta = 9.0$.

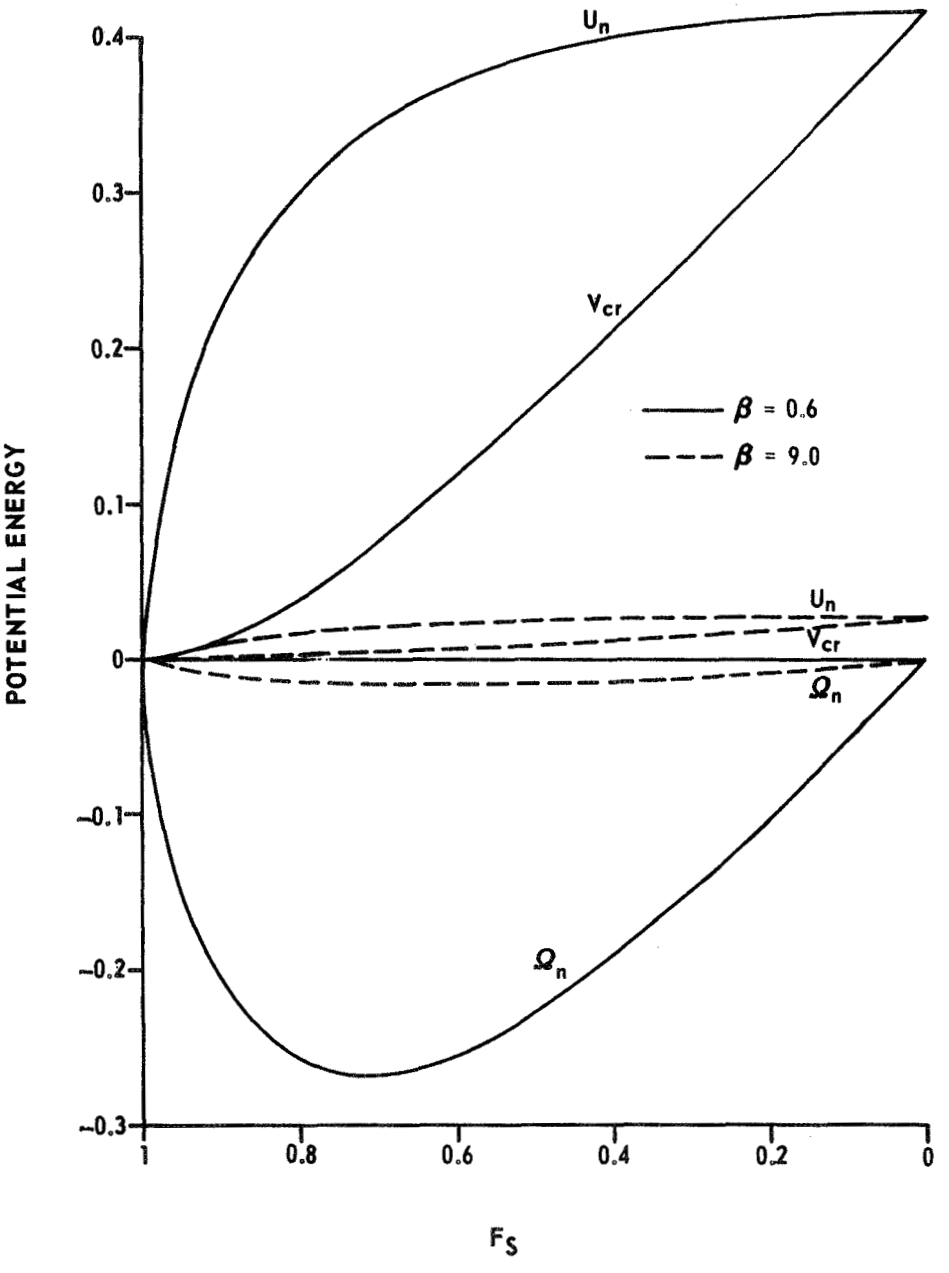

Figure 12. Critical potential energy.

SECTION V. DYNAMICS

A. Method of Analysis

The analyses of Section IV were confined to equilibrium states and a determination of the critical potential energy for these conditions. This section consists of analyses of the dynamic responses to impulsive loads. The impulsive loads considered are of two types:

a. A single square wave such that the impulse, I, is

$$I = F_D \Delta\tau \tag{33}$$

where τ is the nondimensional time of equation (12).

b. A pure impulse where

$$\Delta\tau = 0 \quad .$$

The pure impulse is an initial velocity of φ_1 and/or φ_2 from the equilibrium state without any load being applied. It represents the limit condition

$$I = \lim_{\Delta\tau \to 0} F_D \Delta\tau$$

The use of a pure impulse is necessary because the results would be influenced by the length of $\Delta\tau$ in equation (33). Also the model system of Figure 4 requires an imperfection, ϵ, to initiate motion when loaded with the impulse of equation (33), while the pure impulse will result in movement of the model system without an imperfection.

B. Initial Velocities for Impulsive Loads

When a square-wave impulse is applied to the imperfect system, φ_1 and φ_2 change. The initial velocities of φ_1 and φ_2 can be determined by Lagrange's impulsive equations [5]. Since the system is at rest prior to the impulse, the kinetic energy after the impulse is

$$\frac{\partial T}{\partial \dot{q}_i} = \hat{Q}_i \tag{34}$$

where $\hat{Q}_i$ is the generalized impulse. Using the nondimensional energy equation (15), equation (34) becomes

$$S^2 \left[3\hat{\varphi}_1' + \hat{\varphi}_2' \cos(\varphi_2 + \epsilon_2 - \varphi_1 - \epsilon_1) \right]$$

$$= CF\Delta\tau \, \mathrm{Sin}(\varphi_1 + \epsilon_1) \quad ,$$

$$S^2 \left[\hat{\varphi}_1' \cos(\varphi_2 + \epsilon_2 - \varphi_1 - \epsilon_1) + \hat{\varphi}_2' \right] = CF\Delta\tau \, \mathrm{Sin}(\varphi_2 + \epsilon_2)$$

where $\hat{\varphi}_i'$ is the initial velocity after the impulse. In the initial condition, $\varphi_1 = \varphi_2 = 0$. Using equation (33) and linearizing for ϵ_1 and $\epsilon_2 << 1$, the initial velocities are found to be

$$\hat{\varphi}_1' = \frac{CI}{2S^2} (\epsilon_1 - \epsilon_2) \quad , \tag{35a}$$

$$\hat{\varphi}_2' = \frac{CI}{2S^2} (3\epsilon_2 - \epsilon_1) \quad , \tag{35b}$$

where $I = F_D \Delta\tau$ and $S^2 = \frac{7 - \sqrt{41}}{4}$. Therefore, the initial velocities are dependent on the imperfections in the system as well as the impulse. This also shows, as previously stated, that an imperfection is required for the model to move with an impulse as

$$\hat{\varphi}_1' = \hat{\varphi}_2' = 0 \quad \text{if} \quad \epsilon_1 = \epsilon_2 = 0 \quad .$$

C. Critical Pure Impulse Velocities

Section IV.C showed that if the system was at rest outside the outermost saddle point equal energy contour line in a region of lower energy, it would collapse. Since the system is conservative, the initial kinetic energy is equated to the saddle point potential energy with the system at rest. Then

$$E_n = T_{nb} = U_{nf} + \Omega_{nf} \quad , \tag{36}$$

where E_n is the total energy, T_{nb} is the initial kinetic energy, and U_{nf} and Ω_{nf} are the final strain energy and the potential energy of the load, respectively, at the saddle point. With equation (32), equation (36) becomes

$$T_{nb} = U_{nf} + \Omega_{nf} = V_{cr} \quad , \tag{37}$$

and the initial kinetic energy required to reach the saddle point energy is equal to the critical potential energy of that saddle point. Since the potential of the external load is a negative value [equation (15)], equation (37) shows that an external load will decrease the initial kinetic energy required to reach the saddle point.

Equation (37) is evaluated first without an external load. Using equation (25) and the energy equation (15) with $F_S = 0$, equation (37) is

$$\begin{aligned} &\frac{S^2}{2\beta}\left[3\left(\hat{\eta}_1'\right)^2 + 2\hat{\eta}_1'\hat{\eta}_2' + \left(\hat{\eta}_2'\right)^2\right] \\ &= \frac{1}{4\beta}\left[2\eta_1^2 - \eta_1^4 + \left(\eta_2 - \eta_1\right)^2 - \left(\eta_2 - \eta_1\right)^4\right] \end{aligned} \tag{38}$$

Transposing and setting η_1 and η_2 at any of the saddle points of Figure 7, equation (38) becomes

$$3\left(\hat{\eta}_1'\right)^2 + 2\hat{\eta}_1\hat{\eta}_2' + \left(\hat{\eta}_2'\right)^2 = \frac{1}{2S^2} \tag{39}$$

In the φ coordinate system, this is

$$3\left(\hat{\varphi}_1'\right)^2 + 2\hat{\varphi}_1'\hat{\varphi}_2' + \left(\hat{\varphi}_2'\right)^2 = \frac{1}{2\beta S^2} \tag{40}$$

Solution of this gives the critical pure impulse velocities for initial kinetic energies that will equal the saddle point energy under the conditions

$$F_S = F_D = 0 \quad .$$

The solution of equation (39) is the locus of points shown in Figure 13. This locus of points is an ellipse with the major axis rotated 22.5 degrees from the vertical.

Addition of an external load would change the saddle point and reduce the energy level on the right side of equation (39). Thus, the solution for the initial pure impulse critical values would be a series of concentric ellipses within that shown in Figure 13, with the actual ellipse dependent on F_S.

D. Critical Imperfections

The relationship between the imperfections or eccentricities ϵ_1 and ϵ_2 and the critical impulse I_{cr} to reach the saddle point energy can be determined by substituting equation (35) into equation (40) to get

$$\epsilon_1^2 - 2\epsilon_1\epsilon_2 + 3\epsilon_2^2 = \frac{S^2}{\beta C^2 I_{cr}^2} \tag{41}$$

where S^2 and C are constants with the values previously determined. The solution of equation (41) is a locus of points dependent on the value of I_{cr}.

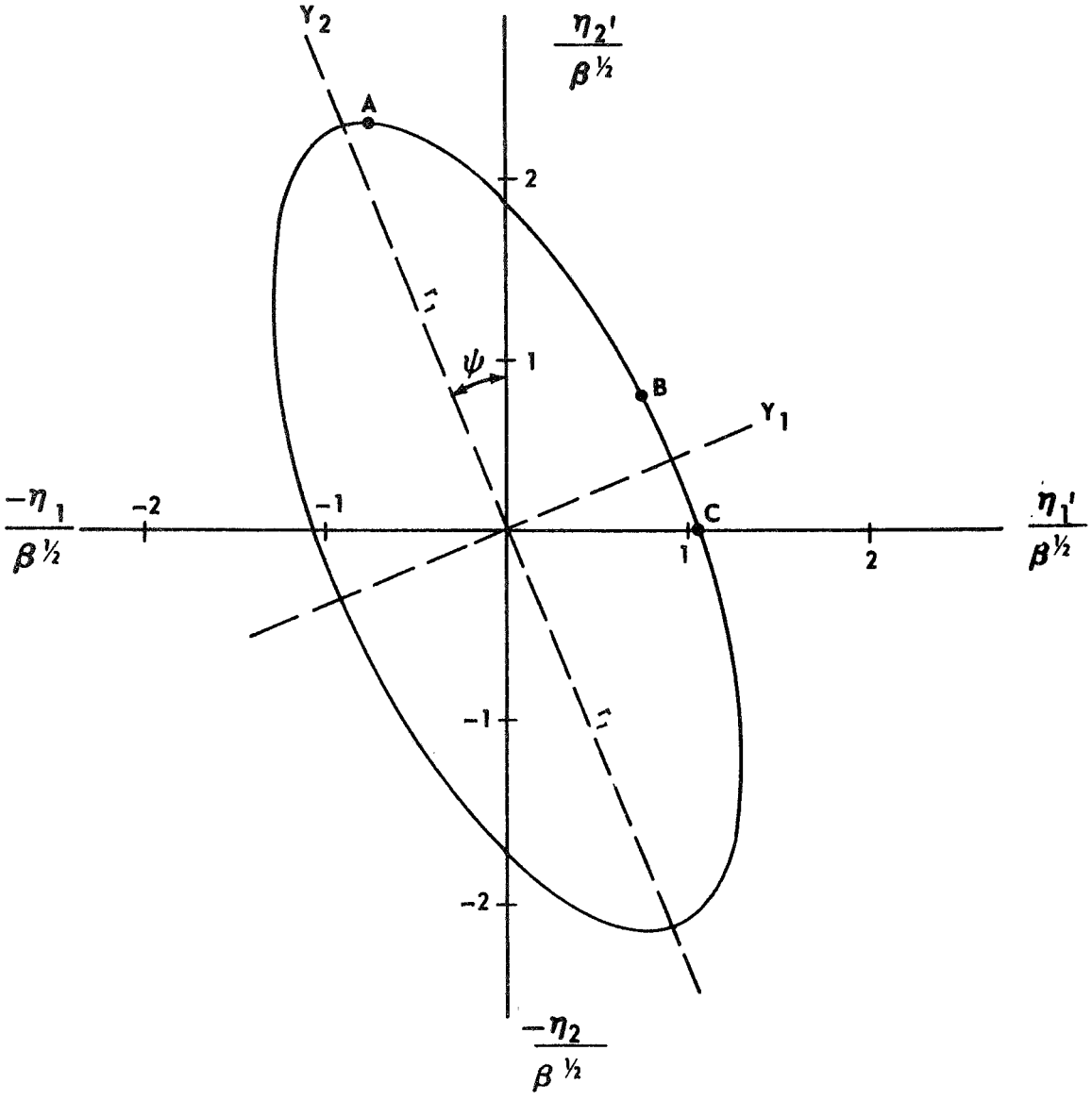

Figure 13. Critical pure impulse velocity when $F_S = 0$.

Figure 14 shows the solution for the value $I_{cr} = 1064$. These solutions are also ellipses at an angle of 22.5 degrees from the coordinate system, and have the same eccentricity as that of Figure 13.

Equation (41) and Figure 14 are based on the condition $F_S = 0$. If an external load is applied to the system, the energy level of the saddle is

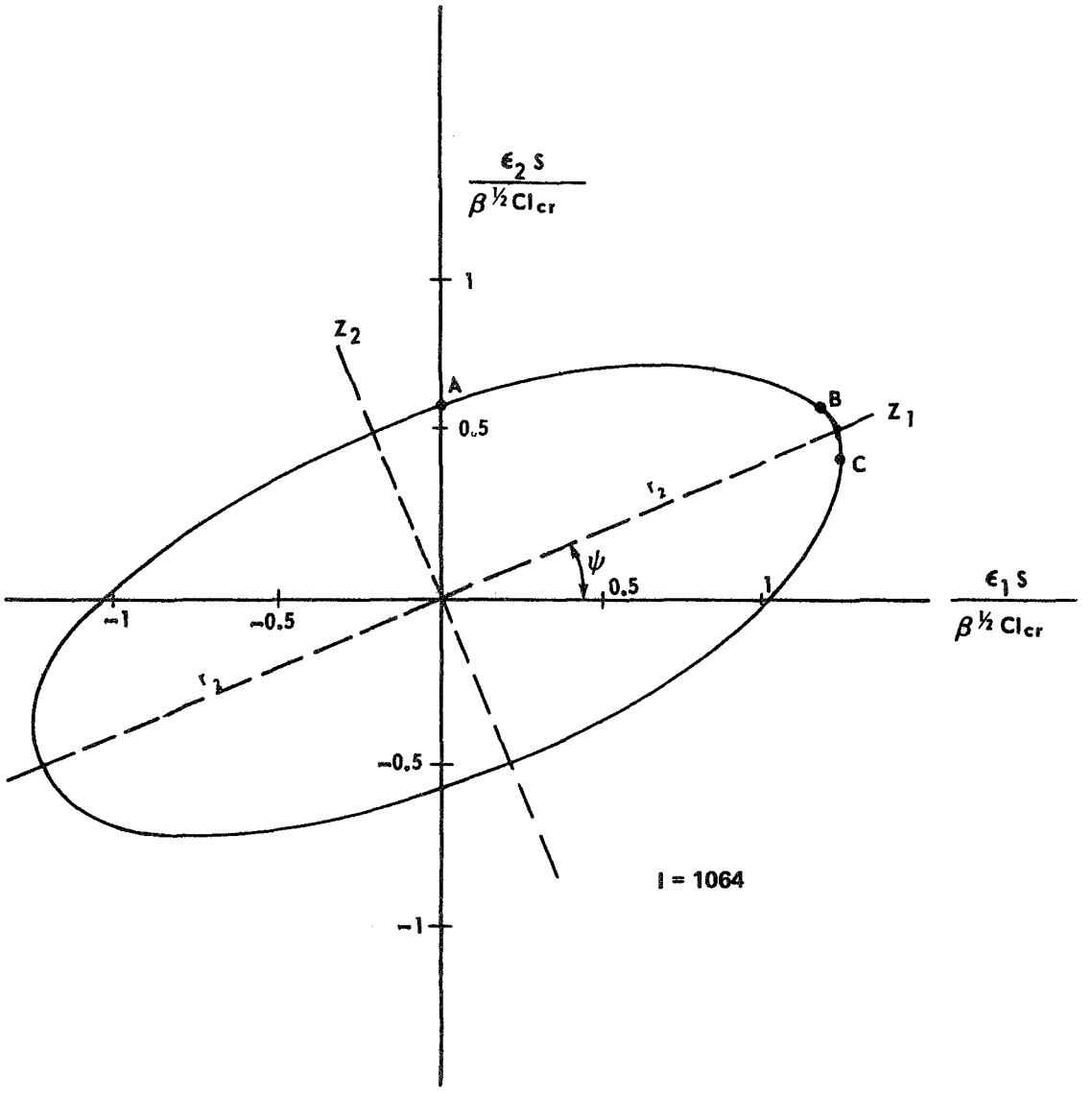

Figure 14. Critical impulse for imperfections of the system.

reduced. Thus, the right side of equation (41) would be reduced and the solution would be a series of concentric ellipses within that of Figure 14, with the actual ellipse dependent on F_S. Points outside the ellipse result in increased kinetic energy.

Equation (41) gives the values of the imperfections in ϵ_i that will cause the system to reach the saddle point energy level for specified values of the spring softner, β, and the applied impulse, I. It can be seen that as the spring softens (β increases) or the impulse increases, the critical values of the imperfections will decrease, as intuitively expected. To

determine the critical impulse to reach the saddle point energy level for specified imperfections, equation (41) is rearranged as

$$I_{cr} = \frac{S}{C\beta^{1/2}(\epsilon_1^2 - 2\epsilon_1\,\epsilon_2 + 3\epsilon_2^2)^{1/2}}$$

E. Relation of Pure Impulse Velocities to the Imperfect System

The relation between the pure impulse velocity in Figure 13 and the velocities of the imperfect system given by the Lagrange impulsive equations can be obtained. For any given conditions of the imperfection ϵ_1 and ϵ_2, a relationship is established for $\hat{\varphi}_1'$ and $\hat{\varphi}_2'$ by equation (35). This can be defined as

$$\hat{\varphi}_2' = K_j \hat{\varphi}_1' \qquad , \qquad j = 1,\ 2,\ 3, \ldots$$

Converting this by equation (25) to

$$\hat{\eta}_2' = K\hat{\eta}_1'$$

and substituting into equation (39) will give a solution corresponding to a point on Figure 13. For example, let $\epsilon_1 = 0$ and $\epsilon_2 = \xi$, an arbitrary value. Then from equation (35)

$$\hat{\varphi}_1' = -\frac{CI}{2S^2}\,\xi \qquad , \qquad \hat{\varphi}_2' = 3\frac{CI}{2S^2}\,\xi$$

and

$$\hat{\varphi}_2' = -3\,\hat{\varphi}_1' \qquad \text{or} \qquad \hat{\eta}_2' = -3\hat{\eta}_1' \qquad (42)$$

Solving equation (39) with equation (42) will give the values of point A on Figure 13. In a similar manner, point B corresponds to $\epsilon_2 = \frac{1}{2}\epsilon_1$, and

point C to $\epsilon_2 = \frac{1}{3}\,\epsilon_1$. Figure 15 shows representative configurations for selected points on the ellipse. In this manner, a pure impulse velocity can be determined that will represent an imperfect system without the distortion introduced in the equations of the imperfect system.

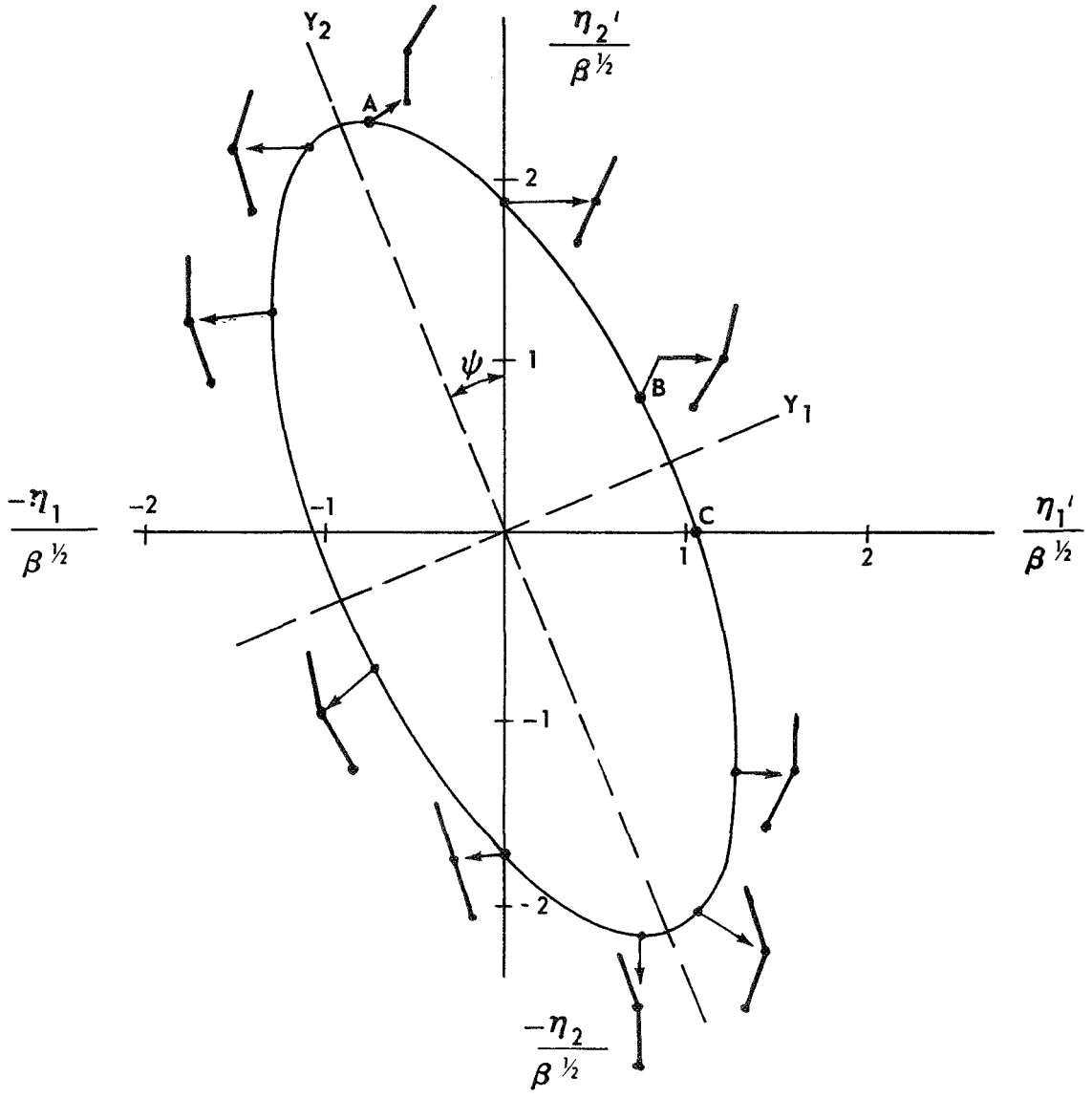

Figure 15. Configurations represented by pure impulses.

Figure 14 is based on the solution of an equation using the imperfections ϵ_1 and ϵ_2 of the system. It has already been shown that Figure 13 can be related to imperfections so there is a correspondence between Figures 13 and 14 and a transformation of coordinates can be established. This transformation is

$$z_1 = G_1 y_1 \quad ,$$

$$z_2 = G_2 y_2$$

where

$$G_1 = \frac{S^2}{I\ C\beta^{1/2}} \left[\frac{2(1 - \cos 2\psi)}{1 + \cos 2\psi}\right]^{1/2} \quad ,$$

$$G_2 = \frac{S^2}{I\ C\beta^{1/2}} \left[\frac{2(1 + \cos 2\psi)}{1 - \cos 2\psi}\right]^{1/2}$$

The transformed locations of points A, B, and C of Figure 13 are shown on Figure 14.

F. Responses to Impulsive Loads

To determine the actual responses to impulsive loads, the nondimensional equations of motion (13) were programmed for the Univac 1108 using a fourth-order Runge-Kutta integration. The different values of F_S and β were used with pure impulse velocities determined from equation (40) that would give the system an initial kinetic energy equal to the saddle point energy. Plots of the responses of the system to these loads and impulses are shown in Figures 16 through 21 for a spring softner constant $\beta = 0.6$.

The solid lines of Figures 16, 17, and 18 show the response with $F_S = 0$ to the initial velocity of points A, B, and C of Figure 13, respectively. In none of these does the configuration reach a point outside the saddle point energy contour.

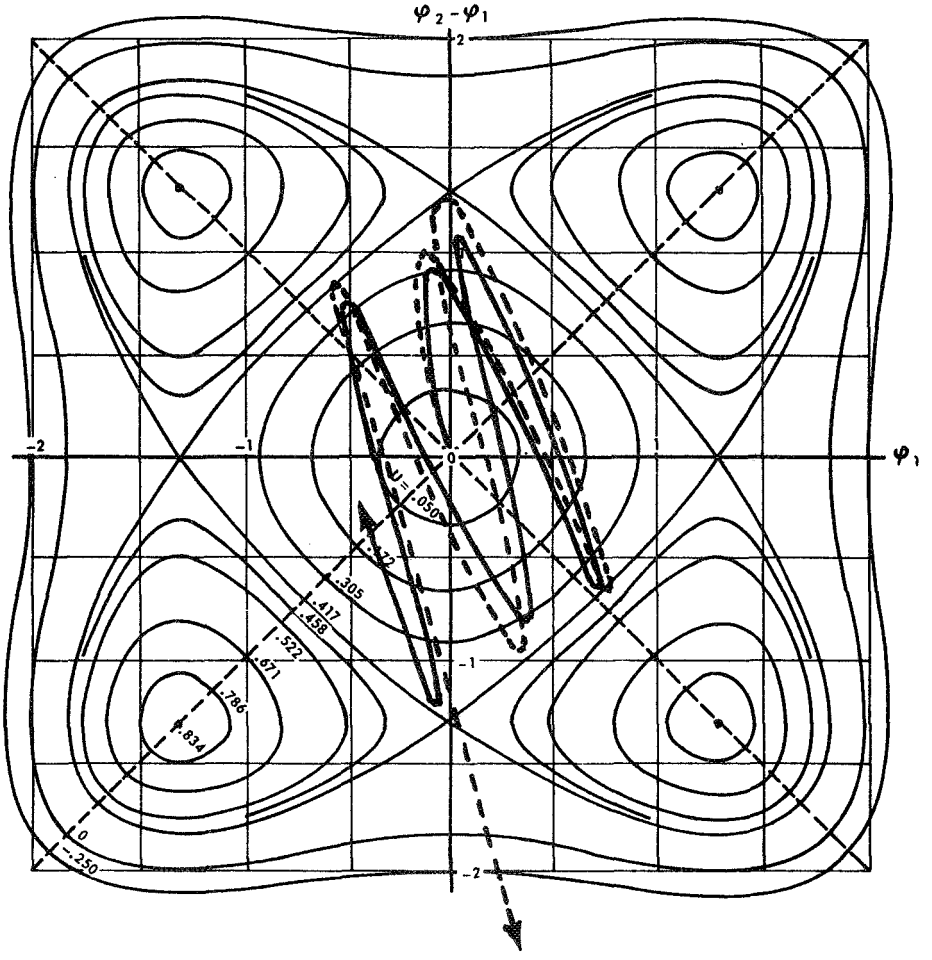

$\beta = 0.6$

——— Initial kinetic energy to reach saddle potential energy.

------ Initial kinetic energy plus 6 percent.

Figure 16. Response of point A to pure impulse ($F_S = 0$).

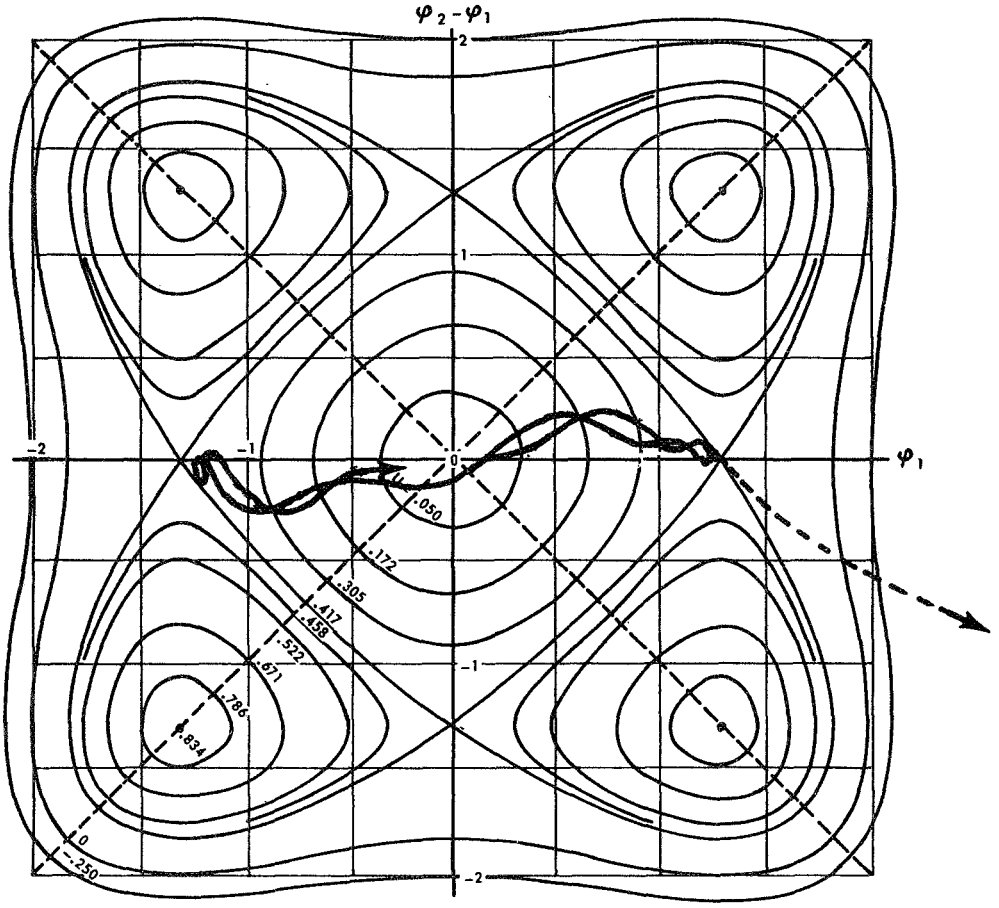

$\beta = 0.6$

——— Initial kinetic energy to reach saddle potential energy.

------ Initial kinetic energy plus 2 percent.

Figure 17. Response of point B to pure impulse ($F_S = 0$).

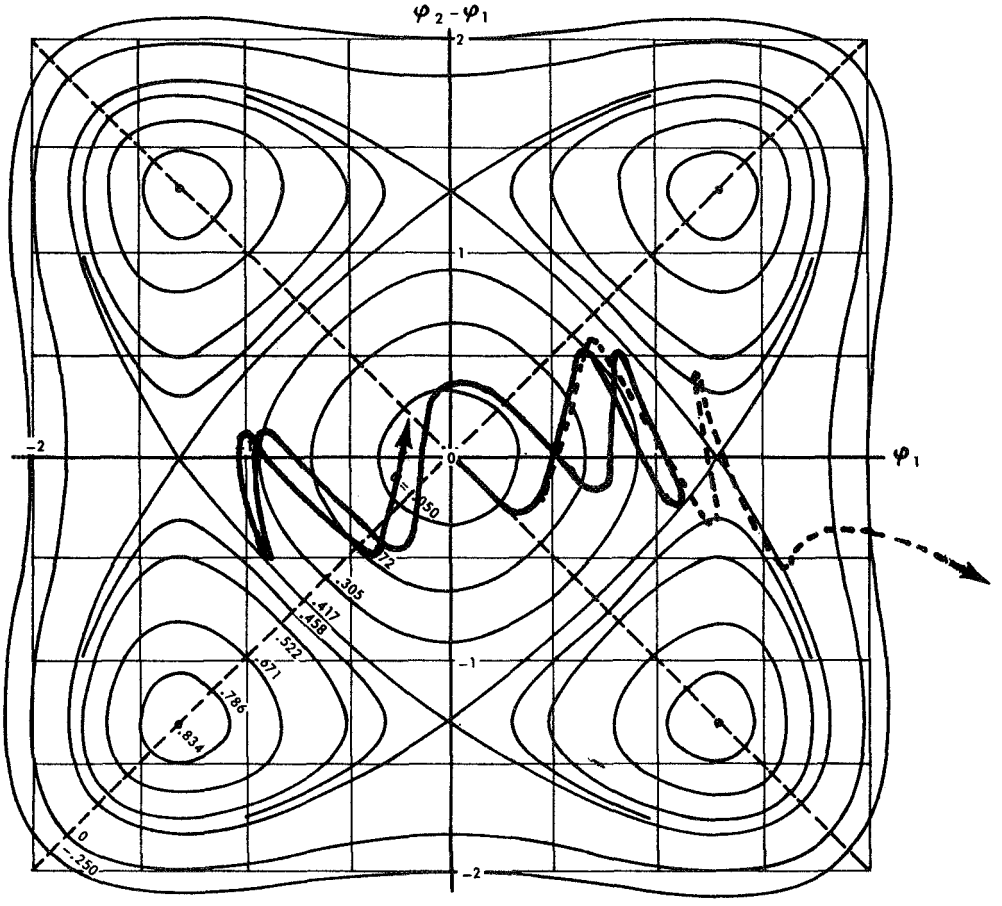

$\beta = 0.6$

——— Initial kinetic energy to reach saddle potential energy.

------ Initial kinetic energy plus 16 percent.

Figure 18. Response of point C to pure impulse ($F_S = 0$).

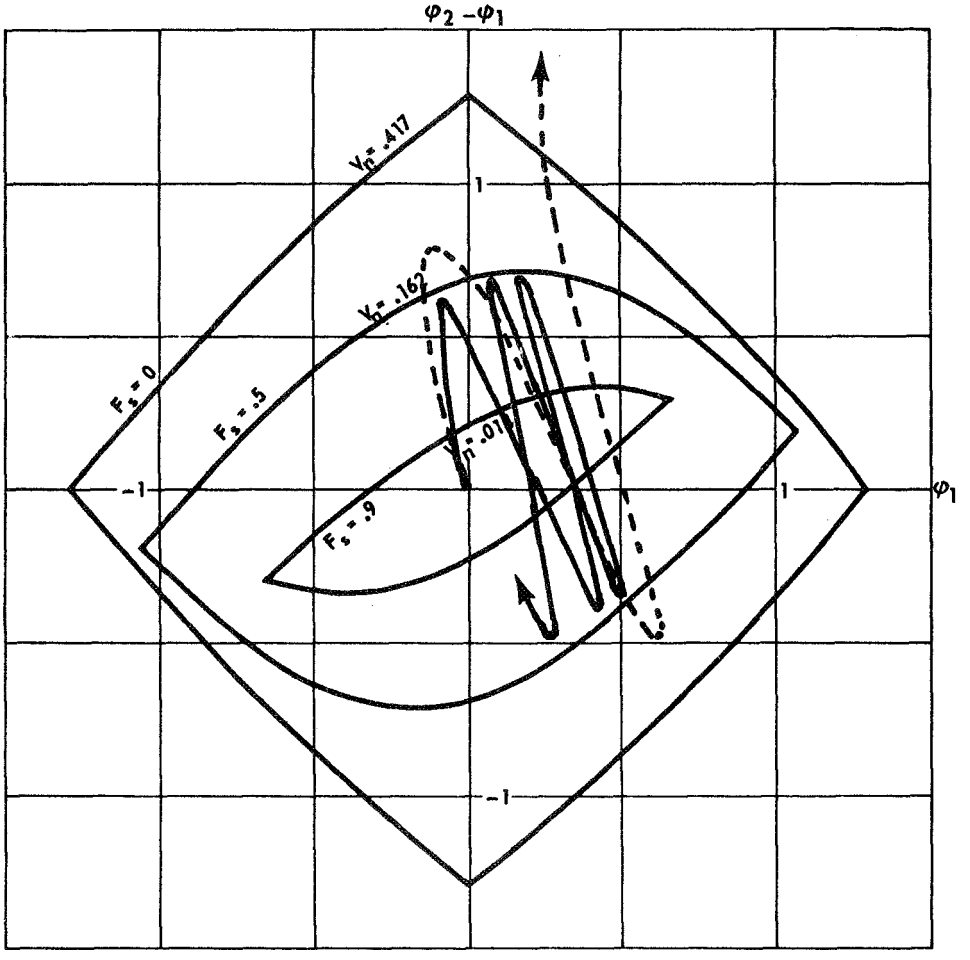

$\beta = 0.6$

——— Initial kinetic energy to reach saddle potential energy.

------ Initial kinetic energy plus 70 percent.

Figure 19. Response of point A to pure impulse ($F_S = 0.5$).

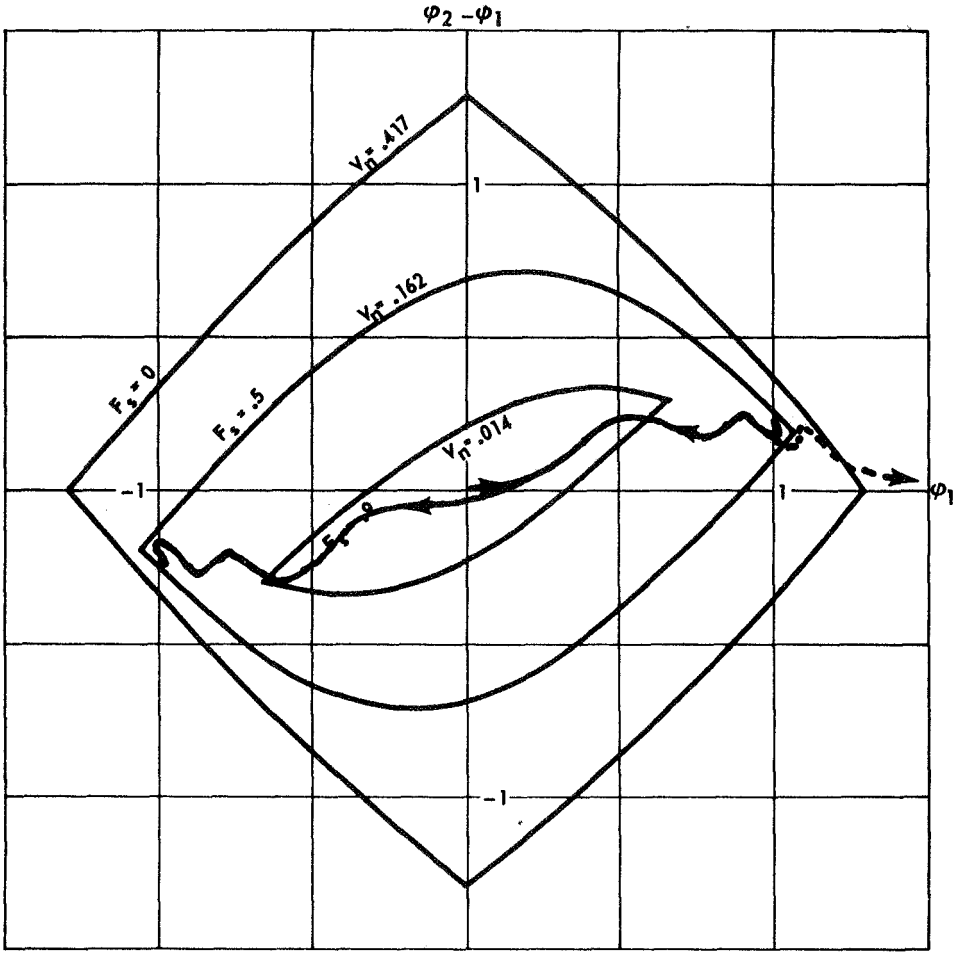

$\beta = 0.6$

——— Initial kinetic energy to reach saddle potential energy.

------ Initial kinetic energy plus 2 percent.

Figure 20. Response of point B to pure impulse ($F_S = 0.5$).

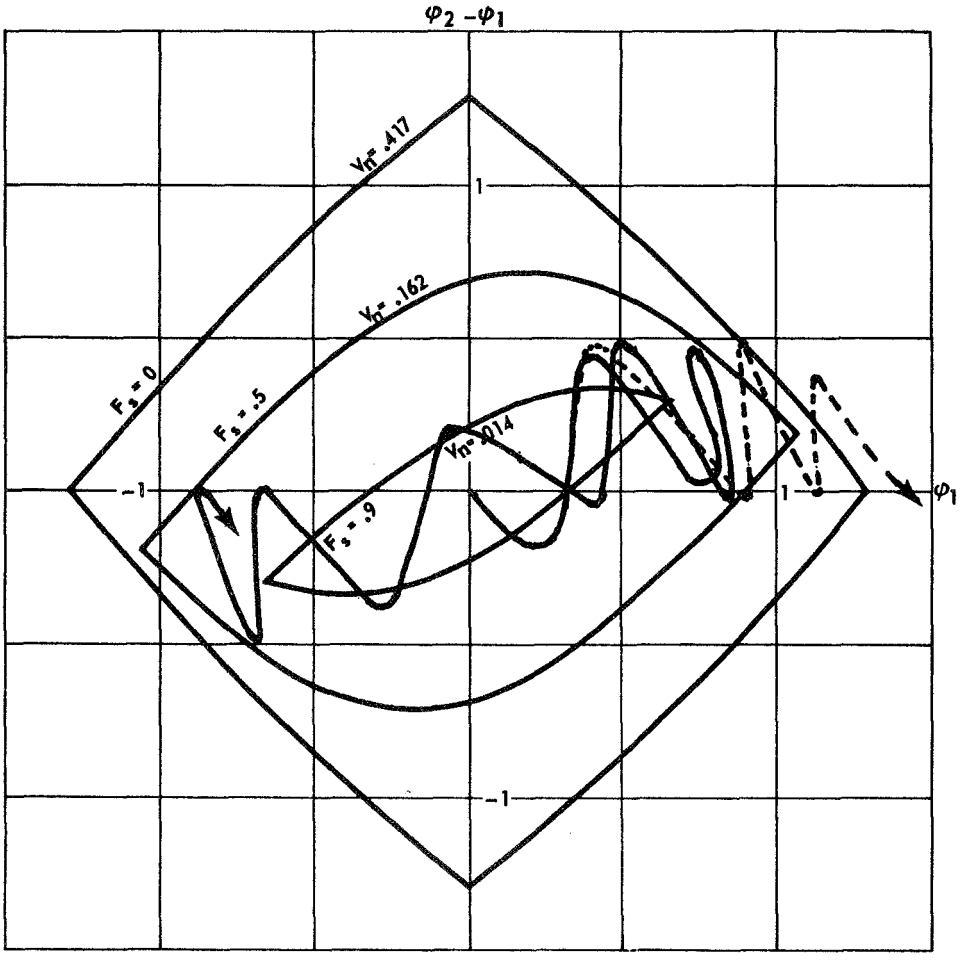

β = 0.6

——— Initial kinetic energy to reach saddle potential energy.

------ Initial kinetic energy plus 20 percent.

Figure 21. Response of point C to pure impulse (F_S = 0.5).

A static load, $F_S = 0.5$, was then applied to the system. The responses are shown by the solid lines in Figures 19, 20, and 21, which correspond respectively to the conditions of Figures 16, 17, and 18, with the exception of the added external load. Again, the system does not go outside the saddle point energy contour.

G. Energy Required for Failure

No equation was found to show the excess energy required to drive the system outside the saddle point energy contour and cause the uncontrolled deflection and failure of the system previously discussed. Computer runs were made with increasing initial kinetic energies until failure of the system resulted on the first cycle. The responses are shown by dotted lines in Figures 16 through 21.

For the unloaded configuration, the excess energy required for failure varied from less than 2 percent for point B of Figure 14 to almost 16 percent for point C. For the system loaded at $F_S = 0.5$, the excess energy varied from less than 2 percent for point B to nearly 70 percent for point A. The excess energy required to make the system fail appears to be related to the direction the system initially moves, being lower when it moves directly toward a saddle.

Several of the points of extreme deflection for the systems with excess energy in Figures 16 through 21 are outside the saddle point energy contour, but in regions of higher energy. Failure only occurs when it is outside this contour in a region of lower energy. Because of computer time limitations, none of these systems was run long. Without dissipation, it is probable that if they ran long enough, all would get in a position where they would fail. Figure 16 shows an example of this, as the system did not go over the saddle on the approach to $+(\varphi_2 - \varphi_1)$, but did at $-(\varphi_2 - \varphi_1)$. Failure of the system in Figure 19 is over the saddle point of position II, which is at a higher energy level than position I. A longer run at a lower energy level might put it over the saddles shown on the contour plot. However, since all real systems have some dissipation energy, early failure is considered a better measure of stability.

SECTION VI. CONCLUSIONS

These analyses were conducted with the nondimensional parameters β, ϵ_i, F, and I to determine their effect on the system, and the major conclusions are contained in Paragraphs A through D below. The dimensional parameters k, l, and m were not explicitly considered; however, some general comments concerning them are contained in Paragraph E. Areas for additional study are listed in Paragraph F.

A. Effect of β

The spring softening term, β, affects the response in three ways:

1. Under static loading, values of β greater than the critical value $\left[\beta_{cr} = \frac{3+\sqrt{5}}{12}\text{; equation (20)}\right]$ result in unstable equilibrium at the critical buckling load and cause a "snap-through" effect as shown in Figure 5. However, the unloaded deflected system becomes unstable at the saddle point at a different value of $\beta\left(\beta < \frac{1}{\pi^2}\text{ ; Fig. 8}\right)$.

2. The location of the saddle point is an inverse function of $\beta^{1/2}$ [equation (24)], and increasing β moves the saddle point toward the origin (Fig. 7), which reduces the amount the system can deflect prior to collapse. Also, an increase in β decreases the energy of the deflected springs [equation (23)] and the critical potential energy (Fig. 12). Since V_{cr} is equal to the energy required to reach the saddle point, an increase in β reduces the dynamic load required to cause collapse.

3. Changing the value of β changes the equation of motion: an increase in β results in greater amplitudes of the two angles and an increase in the period of the system. No analysis of this was made, but the different responses for two inputs, identical except for β, are shown in Figure 22. β_{cr} is not important in the dynamic response as there is little difference in responses for values above and below β_{cr}.

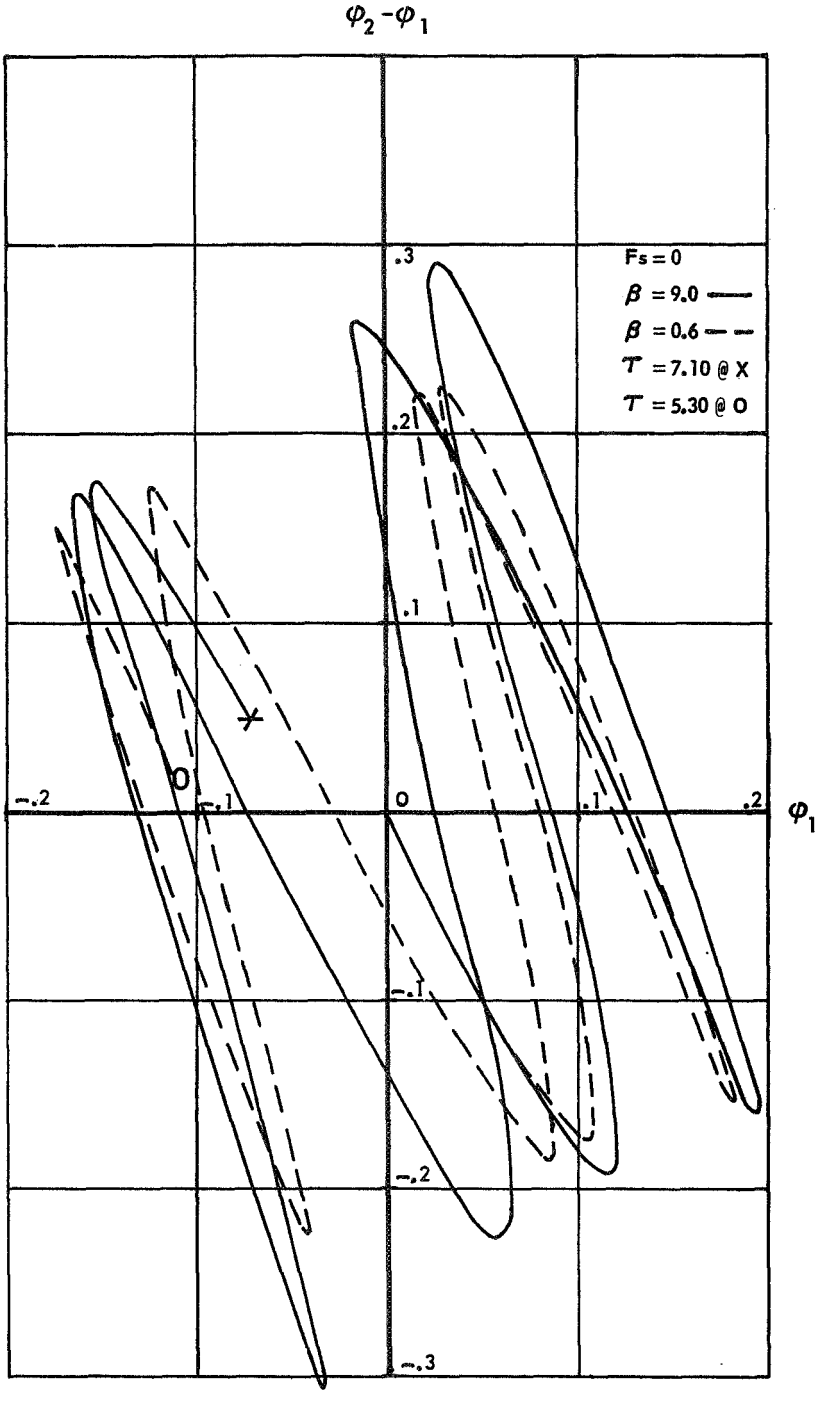

Figure 22. Response with different values of β.

B. Effect of the Imperfection ϵ

1. For the pure impulse (initial velocities of φ_1' and φ_2' equivalent to an impulsive load), the imperfections are not used. However, the initial pure impulse velocities correspond directly to particular imperfections (Section V.E and Fig. 15).

2. The values of ϵ_1 and ϵ_2 that combine with an impulse load to equal the critical potential energy, V_{cr}, and cause collapse are given by the ellipse of Figure 14. For a given impulse, I_{cr}, all values of ϵ_1 and ϵ_2 on the ellipse result in the same initial kinetic energy. Values of ϵ_i within the ellipse will give less energy, and values outside the ellipse will give greater energy and result in collapse of the system.

C. Effect of Static Loading

Increasing the static loading, F_S, decreases the kinetic energy that the system can absorb without collapse [equation (32) and Fig. 12]. This results in smaller concentric ellipses in Figure 13 and reduces the energy pulse required to reach the saddle point energy. Loadings greater than $F_S = 1$ will result in collapse without any initial kinetic energy (provided the model is perturbed slightly from the origin, $\varphi_1 = \varphi_2 = 0$).

D. Effect of Impulses

An initial pulse of energy in excess of V_{cr} will result in the total energy of the system exceeding the saddle point energy, and the system will collapse if it reaches a configuration outside the energy contour of the saddle point and in a region of lower potential energy (Fig. 7). The excess energy required for collapse on the first cycle (a cycle of the system is considered to be the closed path of φ_1) varied from less than 2 percent to 70 percent and is dependent on the initial conditions. As shown in Figures 16 through 21, it is less when the system initially moves directly toward the saddle point. If a static load is applied, a smaller concentric ellipse would give the velocities; however, with a static load, the direction to the saddle changes.

Figures 16 through 21 show that the response of the system to an impulse is an oscillation of the upper angle $(\varphi_2 - \varphi_1)$ in relation to the lower angle (φ_1), while the latter oscillates more slowly. The rapidity of motion of $\varphi_2 - \varphi_1$, in relation to φ_1, is dependent on the initial conditions. Since the response of the system in a configuration space does not trace the same path on each cycle, it is probable that, without a dissipation function, any system with an initial energy in excess of V_{cr} will eventually reach a point where it will collapse.

E. Comments on the Dimensional Parameters

The effect on the system of parameters k, l, and m was not analyzed. However, certain comments can be made concerning them. These parameters are contained in the coefficients of φ_1 and φ_2 in the nondimensional equations and in the term S^2 [equation (12a)].

Changing the assumed mass distribution or making the bars of unequal length (Fig. 4) will change the coefficients of φ_1' and φ_2' in equations (35), (40), and (41). This would change the shape and inclination of the response ellipses in Figures 13 and 14, resulting in different values for the critical impulse. Unequal bar lengths would also change V_{cr} by changing the relation between Ω and U.

In the nondimensional equations, $S^2 = \frac{ml^2\omega^2}{k}$ where ω is the lowest natural frequency of small oscillations. The use of $S^2 = \frac{7 - \sqrt{41}}{4}$ as the lowest natural frequency assumes that $\frac{ml^2}{k} = 1$. Actual values of k, l, and m could change the value of S^2. Assuming the same relationship for m_1, m_2, l_1, and l_2, a change in S^2 would only affect the size of the ellipses in Figures 13 and 14. An increase in S^2 would decrease the ellipse in Figure 13 and result in smaller pure impulse velocities for collapse. This is the same effect as that of an increase in β. It would increase the size of the ellipse in Figure 14 and permit larger imperfections for a given impulse without collapse. This is the opposite effect as that of an increase in β. In other words, a system with a higher natural frequency of small oscillations (stiffer against small displacements) admits smaller impulsive loading, but larger imperfections for a given impulse without collapse. The response for three different values of S^2 is shown in Figure 23.

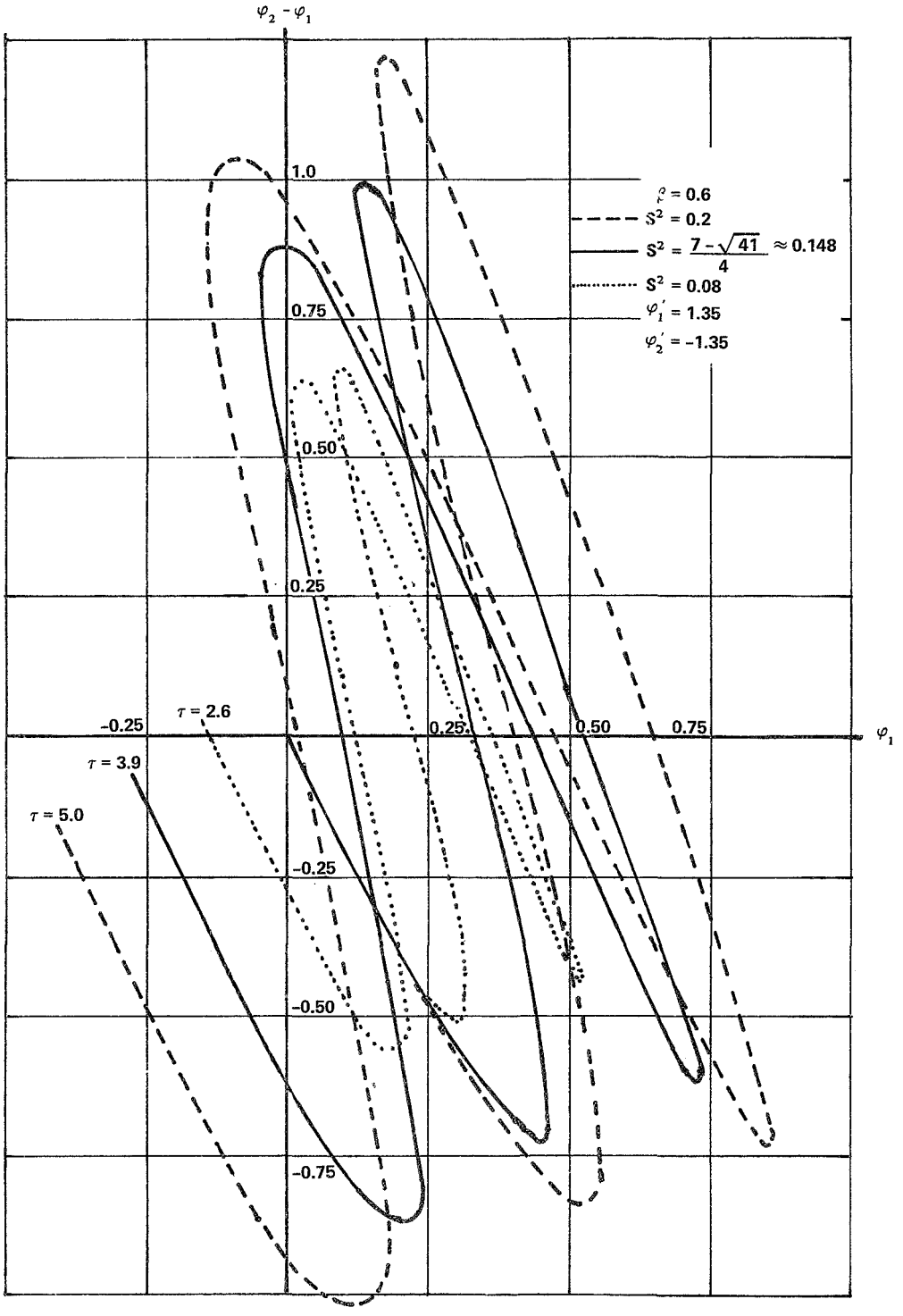

Figure 23. Response with different values of S^2 .

The dimensional parameters discussed in this paragraph only affect the quantitative values of the analyses and do not change the conclusions.

F. Areas for Additional Study

The following are areas where additional analyses would be desirable:

1. The applicability of the nonlinear equations to very small deflections. This includes the effect of β on collapse when the saddle point is near the origin.

2. Further analysis of the effect of β on the system.

3. The effects of S^2 and the different dimensional parameters on the system.

4. The effect of the various parameters on β_{cr}.

5. The applicability of phase-plane trajectories to the analysis.

6. The excess energy requirements for failure after a number of cycles and the effect of the direction of initial displacements.

7. The extension of this concept to multi-degree-of-freedom systems.

8. Introduction of dissipation forces.

G. Applicability to Physical Systems

These analyses are initial theoretical investigations of a simplified system to determine methods that can be used in stability analyses. Further studies as outlined above are needed to determine the effectiveness of the methods as the system deflections approach linearity or the system becomes more complicated (i.e., more degrees of freedom). Because of the assumption of frictionless pins and the use of nondimensional quantities, direct application of the completed analyses to physical systems is not possible. Introduction of dissipation forces at the pins and conversion of the equations to dimensional form (or correlation of dimensional characteristics with the numerical values of the nondimensional equations as discussed in paragraph VIE) is required to make the analyses applicable to physical systems.

REFERENCES

1. Koiter, W. T.: Elastic Stability and Post-Buckling Behavior. Nonlinear Problems. Proceedings of a Symposium at the University of Wisconsin. Edited by Rudolph E. Langer, The University of Wisconsin Press, Madison, Wisconsin, 1963, pp. 265, 260, 262.

2. Langhaar, Henry L.: Energy Methods in Applied Mechanics. John Wiley and Sons, Inc., New York, N.Y., 1962, pp. 30, 32, 308.

3. Goldstein, Herbert: Classical Mechanics. Addison-Wesley Publishing Company, Inc., Reading, Mass., 1959, p. 18.

4. Koiter, W. T.: On the Stability of Elastic Equilibrium. (H. J. Paris, Amsterdam, 1945). Translated by the National Aeronautics and Space Administration, 1967, pp. 119-27.

5. Thomson, William T.: Introduction to Space Dynamics. John Wiley and Sons, Inc., New York, N.Y., 1961, p. 283.

BIBLIOGRAPHY

Books

Myklestead, Nils O.: Engineering Mechanics. Charles E. Merrill Books, Inc., Columbus, Ohio, 1965.

Noble, Ben: Applied Linear Algebra. Prentice Hall, Inc., Englewood Cliffs, N. J., 1969.

Pletta, Dan H.; and Frederick, Daniel: Engineering Mechanics. The Ronald Press Company, New York, N. Y., 1964.

Scarborough, James B.: Numerical Mathematical Analysis. The Johns Hopkins Press, New York, N. Y., 1962.

Tse, Francis S.; Morse, Ivan E.; and Hinkle, Roland T.: Mechanical Vibrations. Allyn and Bacon, Inc., Boston, Mass., 1963.

Voltera, Enrico; and Zachmanoglou, E. C.: Dynamics of Vibration. Charles E. Merrill Books, Inc., Columbus, Ohio, 1965.

Zwikker, C.: The Advanced Geometry of Plane Curves and Their Applications. Dover Publications, Inc., New York, N. Y., 1963.

Articles

Budiansky, Bernard; and Hutchinson, John W.: Dynamic Buckling of Imperfection-Sensitive Structures. Applied Mechanics. Proceedings of the Eleventh International Congress of Applied Mechanics, Munich, Germany (1964), 1966, pp. 636-51.

Budiansky, Bernard; and Hutchinson, John W.: A Survey of Some Buckling Problems. American Institute of Aeronautics and Astronautics Journal, Volume 4, Number 2, September 1966, pp. 1505-10.

Friedrichs, K. O.; and Stoker, J. J.: Forced Vibrations of Systems with Nonlinear Restoring Force. Quarterly of Applied Mathematics, Volume I, Number 2, July, 1943, pp. 97-114.

BIBLIOGRAPHY (Concluded)

Herrman, G.; and Bungay, R. W.: On the Stability of Elastic Systems Subjected to Nonconservative Forces. Journal of Applied Mechanics, Transactions of the American Society of Mechanical Engineers, Volume 31, September 1964, pp. 435-40.

Herrman, G.; and Jong, Ing-Chang.: On the Destabilizing Effect of Damping in Nonconservative Elastic Systems. Journal of Applied Mechanics, Transactions of the American Society of Mechanical Engineers, Volume 32, September 1965, pp. 592-7.

Herrman, G.; and Jong, Ing-Chang.: On Nonconservative Stability Problems of Elastic Systems with Slight Damping. Journal of Applied Mechanics, Transactions of the American Society of Mechanical Engineers, Volume 33, March 1966, pp. 125-33.

Hutchinson, John W.; and Budiansky, Bernard: Dynamic Buckling Estimates. American Institute of Aeronautics and Astronautics Journal, Volume 4, Number 3, March 1966, pp. 525-30.

Pearson, Carl E.: General Theory of Elastic Stability. Quarterly of Applied Mathematics, Volume XIV, Number 2, July 1956, pp. 133-44.

Thompson, J. M. T.: Dynamic Buckling Under Step Loading. Dynamic Stability of Structures. Proceedings of an International Conference held at Northwestern University, Evanston, Illinois, October 18-20, 1965. Edited by G. Herrman, 1966, pp. 215-36.

APPROVAL

STABILITY OF A TWO-DEGREE-OF-FREEDOM SYSTEM WITH STATIC AND IMPULSIVE LOADING

By Mitchell Cash

The information in this report has been reviewed for security classification. Review of any information concerning Department of Defense or Atomic Energy Commission programs has been made by the MSFC Security Classification Officer. This report, in its entirety, has been determined to be unclassified.

This document has also been reviewed and approved for technical accuracy.

C. C. Hagood

C. HAGOOD
Chief, Skylab Systems Division

W. Haeussermann

W. HAEUSSERMANN
Director, Central Systems Engineering

MSFC—RSA, Ala

DISTRIBUTION

DIR
Dr. Rees

DEP-T
Mr. Neubert

PD-DO-SI
Mr. Darwin

PD-MP-A
Mr. Guffin

PD-SA-V
Mr. Orillion

S&E-DIR
Dr. McDonough

S&E-AERO-DO
Mr. Rheinfurth

S&E-ASTN-A
Mr. Sterett

S&E-ASTN-AS
Mr. Coldwater

S&E-CSE-DIR
Dr. Haeussermann

S&E-CSE-A
Mr. Cash (20)

AD-S

A&TS-PAT
Mr. L. D. Wofford, Jr.

CC-P
PM-PR-M
A&TS-MS-H
A&TS-MS-IP (2)
A&TS-MS-IL (8)
A&TS-TU (6)

Scientific and Technical Information
Facility (25)
P. O. Box 33
College Park, Maryland 20740
Attn: NASA Representative (S-AK/RKT)